INTERNATIONAL GEOLOGY REVIEW
https://doi.org/10.1080/00206814.2024.2315556

Taylor & Francis
Taylor & Francis Group

Tectonic stress around the South Caspian basin deduced from earthquake focal mechanisms

Ahad Nouri[a], Behnam Rahimi[a], Václav Vavryčuk[b] and Farzin Ghaemi[a]

[a]Department of Geology, Faculty of Science, Ferdowsi University of Mashhad, Mashad, Iran; [b]Institute of Geophysics, Czech Academy of Sciences, Prague, Czech Republic

ABSTRACT

In this paper, we study the tectonic stress around the South Caspian Basin (SCB), which includes the Kopeh Dagh, Alborz, Talesh, eastern Greater Caucasus mountain belts, the Apsheron sill, and the Balkhan-Ashkabad fault zone. We apply the stress inversion to focal mechanisms of 410 main-shocks that have occurred over the last 69 years. These mechanisms indicate that the surrounding fault zones of the SCB exhibit diverse types of faulting, ranging from thrust to strike-slip, normal, and their combinations. The results of the stress inversion align with the kinematics of the major fault zones bounding the SCB and emphasize the spatial heterogeneity of the stress field in this region. The region is predominantly under compression, but transpressive and strike-slip regimes are also present. This highlights the role of obliquely oriented basement faults with respect to the maximum horizontal compressive stress (S_{Hmax}) in accommodating deformation through convergent zones. The orientation of the S_{Hmax} is in the NE to NNE direction in the Kopeh Dagh, Alborz, Talesh, and Ashkabad-Balkhan fault zones, being rotated to NNE-N in the Greater Caucasus. The orientation of the S_{Hmax} relative to the convergence direction of the Arabian and Eurasian plates indicates that the Arabian-Eurasian oblique convergence-derived tectonic stress is the primary contributor to the total stress and deformation in this region.

ARTICLE HISTORY
Received 15 April 2023
Accepted 4 February 2024

KEYWORDS
South caspian basin; stress; stress inversion; focal mechanism

1. Introduction

The South Caspian Basin (SCB) is a relatively stable block with a rigid oceanic basement in the northern part of the active Alpine-Himalayan orogenic belt (Figure 1) (Priestley *et al*. 1994; Jackson *et al*. 2002; Allen *et al*. 2003, 2003). The SCB is confined by the Apsheron-Balkhan sill to the north and the continuous arcuate-shaped Talesh-Alborz-Kopeh Dagh fold-and-thrust belt wrapping around it (Figure 1) (Berberian 1983; Jackson *et al*. 2002; Hollingsworth *et al*. 2010; Aziz Zanjani *et al*. 2013; Madanipour *et al*. 2018; Mattei *et al*. 2019). Shortening in this region has been accommodated by folding and oblique left-lateral thrust faulting along the western and southern edges of the South Caspian block (Stöcklin 1974b; Berberian 1983; Allen *et al*. 2003; Hollingsworth *et al*. 2010; Mousavi *et al*. 2013; Madanipour *et al*. 2018; Mattei *et al*. 2019; Naeimi *et al*. 2022).

An overview of the present-day geodynamics of the South Caspian block was provided by Jackson *et al*. (2002). According to Jackson *et al*. (2002), the ENE-WSW-striking left-lateral faulting along the Shahroud fault system in the eastern Alborz to the south and the right-lateral faulting along the NW-SE-striking Ashkhabad fault to the north allow the South Caspian block to extrude westward (Figure 1). The right-lateral and left-lateral slip rate along the Ashkabad fault and the Shahroud fault system at ~ 56°E are estimated by the Global Positioning System (GPS) to be ~ 5 and ~3.7 mm/yr, respectively (Khodaverdian *et al*. 2015; Khorrami *et al*. 2019). The largest portion of the westward motion of the SCB is accommodated by northward subduction of it's basement beneath the North Caspian Basin along the Apsheron-Balkhan sill (Figure 1) (Jackson *et al*. 2002). Shortening along the northern margin of the SCB was estimated to be ~6 mm/yr by Djamour *et al*. (2010). The velocity vector of the SCB at an average rate of ~7 mm/yr (Mousavi *et al*. 2013) changes from N45°W in the south to N in the north relative to Eurasia (Djamour *et al*. 2010).

Approximately from the beginning of Pliocene, the sedimentation rate in the SCB underwent a dramatic increase by about one order of magnitude with a reach in turbidite value due to subsidence of the basin. The subsidence was 1.5–10 times higher than in other typical foreland basins (Nadirov *et al*. 1997; Allen *et al*. 2002). This is interpreted as initiation of the tectonic activity of

CONTACT Ahad Nouri ahad.nouri@mail.um.ac.ir Department of Geology, Faculty of Science, Ferdowsi University of Mashhad, Mashad, Iran
This article has been corrected with minor changes. These changes do not impact the academic content of the article.
Supplemental data for this article can be accessed online at https://doi.org/10.1080/00206814.2024.2315556

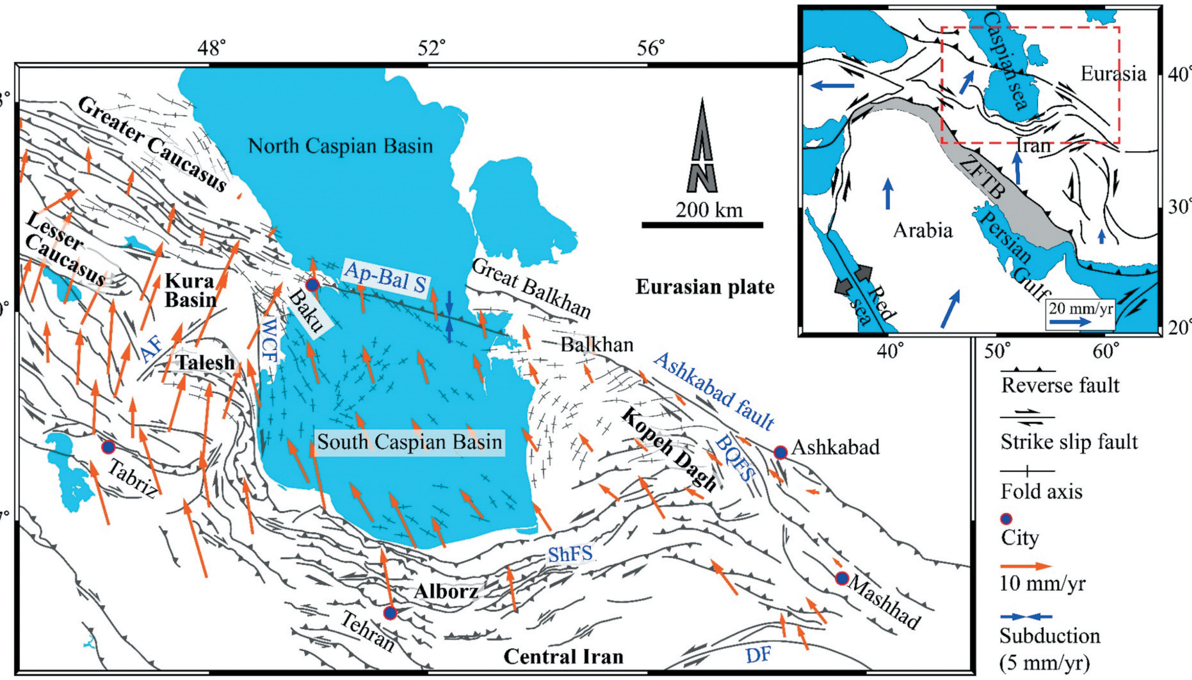

Figure 1. Structural map of the study area (after Ghassemi (2005), Jackson *et al*. (2002), Aziz Zanjani *et al*. (2013), and Nouri Mokhoori *et al*. (2021)). AF: Aras fault, WCF: West Caspian fault, DF: Doruneh fault, SHFS: Shahrud fault system, BQFS: Bakharden–Quchan fault system, Ap-Bal S: Apsheron-Balkhan sill. GPS velocities (orang arrows) are relative to Eurasia fixed framework (Tavakoli 2007; Djamour *et al*. 2010, 2011). Inset: tectonic map of the Arabian-Eurasian collision zone (after Nouri *et al*. (2023) and referenes therin). The red rectangle shows the location of the study area. Blue arrows show the GPS-derived plate velocities (mm/yr) relative to Eurasia fixed framework (Reilinger *et al*. 2006). ZFTB: Zagros fold-and-thrust belt.

the SCB (Nadirov *et al*. 1997; Allen *et al*. 2002; Jackson *et al*. 2002; Hollingsworth *et al*. 2008, 2010).

As suggested by current rates of strain inferred from GPS measurements (Khorrami *et al*. 2019), seismotectonic studies (e.g, Jackson and McKenzie 1984; Jackson 1992, 2001; Priestley *et al*. 1994; Jackson *et al*. 2002; Hollingsworth *et al*. 2008, 2010; Aziz Zanjani *et al*. 2013; Nemati *et al*. 2013; Azad *et al*. 2019; Walker *et al*. 2021) show that the SCB is a relatively aseismic block bounded by three seismic zones known as the Alborz, Talesh, and Apsheron-Balkhan-Ashkabad fault zones (Figure 1). The seismicity in these zones is associated with the reactivation of the basement faults in response to the far-field stress that is derived from ~NNE-trending convergence between the Arabian and the Eurasian plates (e.g, Berberian 1983; Priestley *et al*. 1994; Jackson *et al*. 2002; Javidfakhr *et al*. 2011; Aziz Zanjani *et al*. 2013; Nemati *et al*. 2013; Tadayon *et al*. 2019; Tibaldi *et al*. 2020). GPS measurements (Vernant *et al*. 2004; Reilinger *et al*. 2006; Khorrami *et al*. 2019) sustain an oblique convergence between these plates. The rate of the convergence is estimated to ~26 mm/yr at 56°E in the south of Iran (Khorrami *et al*. 2019).

Geology and tectonics of the SCB and its surrounding tectonic domains has been studied by many authors (e.g, Stöcklin 1974a, 1974b; Berberian 1983; Allen *et al*. 2002, 2003, 2003; Brunet *et al*. 2003; Hollingsworth *et al*. 2006, 2008; Guest *et al*. 2007; Hollingsworth 2007; Azad *et al*. 2011, 2019; Madanipour *et al*. 2018; Tibaldi *et al*. 2020; Aflaki *et al*. 2021; Naeimi *et al*. 2022; Trexler *et al*. 2022; Malekzade and Bellier 2023). However, the present-day stress of the region is not well understood. A few studies have locally addressed the stress state in this region being mostly focused on south and southeast of the SCB. Zamani *et al*. (2008) and Shabanian *et al*. (2010) studied the active stress in the Kopeh Dagh fold-and-thrust belt, and Javidfakhr *et al*. (2011) analysed the stress in the central-eastern part of the Alborz, between longitudes 52° and 57°E, based on a limited number of earthquake focal mechanisms (EFMs). Malekzade (2018, 2023) estimated the active stress in the study area, but their results suffer from some deficiencies that will be discussed later.

To thoroughly identify the variation of background stress in this region, we employ considerably larger number of mainshock focal mechanisms than in the previous studies. Additionally, we use an iterative joint stress inversion method that allows to compute more accurate results and to identify which of nodal planes is the fault (Vavryčuk 2011, 2014, 2015). The main purpose of the study is to reveal the active stress field, tectonic regime, orientation of the maximum horizontal compressive stress (S_{Hmax}) and its spatial variation in the study area. In addition, we interpret the stress field in relation to the structural framework of the area.

2. Tectonic setting

The main features of the SCB are the absence of a granitic layer, a relatively high crustal velocity (Vp = 6.6–7.1 km/s) and ocean-like basement, a low seismicity, minor deformation, negative Bouger anomalies, and thick sedimentary cover (up to ~25 km) (Berberian 1983; Priestley *et al*. 1994; Nadirov *et al*. 1997; Allen *et al*. 2002; Jackson *et al*. 2002; Brunet *et al*. 2003; Granath *et al*. 2007; Guest *et al*. 2007; Hollingsworth *et al*. 2008). The origin of the SCB is not well understood. Stöcklin (1974b) considered the SCB as a remnant of the northern Paleotethys. Berberian (1983) believed that it may be a part of the Paleozoic-Triassic ocean, or a marginal sea behind a Mesozoic-Palaeogene ocean that is survived in the form of the present-day SCB compressional depression. Brunet *et al*. (2003) explained the SCB in the context of a back arc basin that developed in the Middle-Late Jurassic and probably reactivated during Cretaceous (Agard *et al*. 2011). In another interpretation, Adamia *et al*. (1977) proposed that the SCB resulted from a rifting process during Palaeogene. Apol'sky (1974) believed that the SCB and the Black Sea were formed by a sinistral transtensional dynamics at the southeastern and northwestern end of a left-lateral fault, respectively, during Late Jurassic-Early Cretaceous. Şengör (1990) considered the SCB as a pull-apart basin that developed between the large-scale Kopeh Dagh-Alborz and Caucasus-Apsheron-Balkhan strike-slip fault system during Cretaceous time.

Berberian (1983) believed that the uplift of the surrounding mountains of the SCB due to compressional tectonic regime indicated the downward motion of the basin from Cenozoic Era. However, recent studies (Nadirov *et al*. 1997; Allen *et al*. 2002) reveal that the basement of the basin has underwent a flexural subsidence. The subsidence and erosion of the surrounding uplifted area provide an opportunity for sediments to accumulate rapidly in this basin. According to Nadirov *et al*. (1997), the age of the sediments goes back to Jurassic. About 10 km of them have been deposited since Late Miocene and a bulk of them was deposited during the Plio-Quaternary time (Nadirov *et al*. 1997; Allen *et al*. 2002; Brunet *et al*. 2003; Guest *et al*. 2007). Depending on the distribution of the pre-Pliocene sedimentary units in the basin, the SCB contains one or more detachment layers (Allen *et al*. 2003). The detachment horizons allow the sedimentary cover to deform into buckle folds (Nadirov *et al*. 1997; Allen *et al*. 2002, 2003; Brunet *et al*. 2003). The dramatic increase of the sedimentation since Pliocene was interpretated as a result of the Plio-Quaternary subsidence of the basin due to initiation of the subduction and underthrusting of the south Caspian basement beneath the northern and western margins, respectively (Nadirov *et al*. 1997; Jackson *et al*. 2002; Allen *et al*. 2002, 2003). Jackson *et al*. (2002) and Hollingsworth *et al*. (2008) proposed that roughly westward extrusion of the West Kopeh Dagh-SCB between the right-lateral Ashkabad and left-lateral Shahrud fault systems enforces the basement of the SCB to northward subduction along a thrust fault, roughly coinciding with the Apsheron-Balkan sill. Jackson *et al*. (2002) suggested that the absence of seismicity in the north of the thrust fault at depths greater than 100 km implies that the subduction has not yet progressed far.

The Talesh-Alborz-Kopeh Dagh belt (TAKB) has experienced long-term polyphase tectonic events over the time (e.g., Stöcklin 1974a, 1974b; Berberian and King 1981; Şengör 1990; Ritz *et al*. 2006; Hollingsworth *et al*. 2010; Chu *et al*. 2021). Although the Pan-African ductile deformation is reported for the region (Chu *et al*. 2021), Precambrian of the belt is not well known (Berberian and King 1981). Tectonically, this region is a result of the Eo-Cimmerian orogeny and the Late Mesozoic inversion of the Early Mesozoic extensional system (e.g, Berberian and King 1981; Lyberis 1999; Madanipour *et al*. 2018; Naeimi *et al*. 2022). The basement of the region is overlain by a thick sediment cover, ranging in age from the Late Neoproterozoic-Cambrian to Quaternary, mostly deposited in a subsiding marine environment (e.g, Berberian and King 1981; Allen *et al*. 2003; Chu *et al*. 2021). This region underwent a calc-alkaline magmatic activity, deformation, and sedimentation during Paleozoic Era (Berberian and King 1981). Rifting of the basement took place during Late Ordovician and Silurian. The extensional phase lasted presumably to upper Devonian-lower Carboniferous. The resulting ocean known as Paleo-Tethys reached its highest width at this time (Berberian and King 1981; Chu *et al*. 2021). The northward motion of the Iranian plate due to opening of the Neo-Tethys Ocean along the Main Zagros thrust fault enforced the Paleo-Tethys to northward subduction during Permian and consequently closer to the ocean in the Triassic period (e.g, Berberian and King 1981; Muttoni *et al*. 2009; Madanipour *et al*. 2018; Chu *et al*. 2021). During Middle Jurassic, post-collisional subsiding basins were produced due to stretching along the basement normal faults (Berberian and King 1981; Lyberis 1999; Allen *et al*. 2003; Robert *et al*. 2014; Madanipour *et al*. 2018; Chu *et al*. 2021; Naeimi *et al*. 2022). The subsidence is highlighted by ~7 km-thick sedimentary successions accumulated in the Kopeh Dagh basin during Middle Jurassic-Tertiary (Berberian and King 1981; Lyberis 1999; Robert *et al*. 2014). Due to the collision of the Arabian and Iranian plates during Late Cretaceous-Paleocene, the crust of Iran underwent a NE to NNE-trending compressional tectonic regime. The compression enforced the extensional tectonic of the TAKB, causing it to invert from normal to thrust kinematics. Subsequently, there was shortening and uplift of the belt through thrusting and folding (Berberian and King 1981; Allen *et al*. 2003; Madanipour *et al*. 2018). The overall structure of the region is (sub)parallel to the Paleotethys suture zone at present, implying the importance of the inherited geological structure in the future structural evolution of this region (Berberian and King 1981; Lyberis 1999; Hollingsworth 2007, 2010; Robert *et al.* 2014). Geological studies (Lyberis 1999; Madanipour *et al.* 2018; Naeimi *et al*. 2022) show that the uplift in different parts of the belt did not occur simultaneously. Studies of the thermal history (Rezaeian *et al*. 2012) indicate that a major acceleration of exhumation in the central Alborz initiated in the Middle Eocene (35 ± 5 Ma) and Late Miocene to Early Pliocene (from 17 ± 2 to 6 ± 1 Ma). Similar results were obtained for the western Alborz at 40 Ma and at 6 Ma (late Miocene-Early Pliocene) (Axen *et al*. 2001). To the east, in the Kopeh Dagh, geological studies indicate significant uplifts during Eocene-Oligocene (Robert *et al*. 2014) and post-Pliocene (Lyberis 1999).

3. Data and method

We compiled available well-constrained EFMs for the study area from: (1) online catalogues including Centroid Moment Tensor catalogue (CMT) (Dziewonski *et al.* 1981; Ekström *et al*. 2012), Iranian Seismological Center (IRSC) (Hosseini *et al*. 2019), International Seismological Centre (ISC) (Lentas 2018; Lentas *et al.* 2019), Kandilli Observatory and Earthquake Research Institute (KOERI) (Cambaz *et al.* 2019), and Zurich Moment Tensors (ZUR_RMT) (Bernardi *et al*. 2004), and (2) published literature (Fara 1964; Jackson and McKenzie 1984; Jackson 1992, 2001; Priestley *et al*. 1994; Gao and Wallace 1995; Jackson *et al*. 2002; Tatar and Hatzfeld 2009; Nemati *et al.* 2011, 2013; Donner *et al.* 2013, 2014; Ansari *et al*. 2015; Yetirmishli *et al*. 2019; Azad *et al*. 2019; Khosravi *et al*. 2019; Hosseini *et al*. 2019; Niksejel et al., 2021; Tibaldi *et al*. 2020; Walker *et al*. 2021). Then, by declustering (Reasenberg 1985) the EFM dataset, we created a catalogue of declustered (mainshock) focal mechanisms containing 410 focal mechanisms of earthquakes with a magnitude ≥2.5 MS (see the Supplementary file). Reasenberg's method (Reasenberg 1985) is a strict space-time declustering approach designed to distinguish background/main events from foreshocks and aftershocks of a region by connecting events into clusters based on adaptive space-time interaction zones. This strategy eliminates events resulting from interactions between faults, and suppresses both spatial and temporal perturbations of stress produced by large earthquakes (Stein 1999; Soh *et al*. 2018; Heidbach *et al*. 2018; Hardebeck and Okada 2018). These earthquakes took place between 1953 and June 2021 with magnitudes (ML) ranging from 2.5 to 7.6. 73% of data are characterized by a depth of less than 20 km and others cover a depth between 20 and 63 km. About the methods used for determining the focal mechanisms see Supplementary file. In this study, the term 'mainshock events' refers to declustered events.

The EFM data set was subdivided into 23 subsets based on the structural patterns and geometry of major faults. For the areas with dense distribution of the focal mechanisms, we applied the *K*-means clustering algorithm (Aggarwal and Reddy 2014) on epicentres of earthquakes. This algorithm classifies *n* earthquakes to *K* clusters regardless of the data similarity and/or associated structural pattern of the earthquake locations. However, it ensures that each earthquake is assigned to a cluster with the nearest centre to the earthquake epicentres. Each of the 23 subsets consisted of at least 10 focal mechanisms (Figure 2) to obtain reliable results (Balfour *et al*. 2011).

For each subset of focal mechanisms, we controlled the homogeneity and/or best-fitting of stress by the following parameters:

(1) Low average deviation angle of the subset. In this study, the computed stress field is assumed homogenous, provided the average deviation between the actual and modelled directions of the slip is lower than 35° (Michael 1991).
(2) Clustered 95% confidence and the value of the stress ratio. Clustered 95% confidence regions of the principal stress axes and/or overlapped 95% confidence regions of σ_1-axis and σ_2-axis with a high stress ratio or overlapped 95% confidence regions of σ_2-axis and σ_3-axis with a low stress ratio.
(3) Stability of the S_{Hmax} orientation. When defining the subsets, we checked repeatedly the S_{Hmax} orientation of subgroups to obtain a stable and well-constrained orientation, which did not change by adding or rejecting mechanism(s).
(4) Homogeneity of the structural pattern. Since the structural pattern of a large-scale region is not homogenous, the focal mechanism data of such region cannot be inverted altogether in term of the homogenous stress state. Hence, to study a regional variation in stress, the target region should be divided into sub-areas.

We determined the type of the focal mechanisms by the plunge angle of their pressure (P), null (B), and tension (T) axes (Frohlich 1992). Inversion of the EFM data for stress is performed by the iterative joint inversion method proposed by Vavryčuk (2014). This method estimates directions of the principal stresses (σ_1, σ_2, and σ_3,

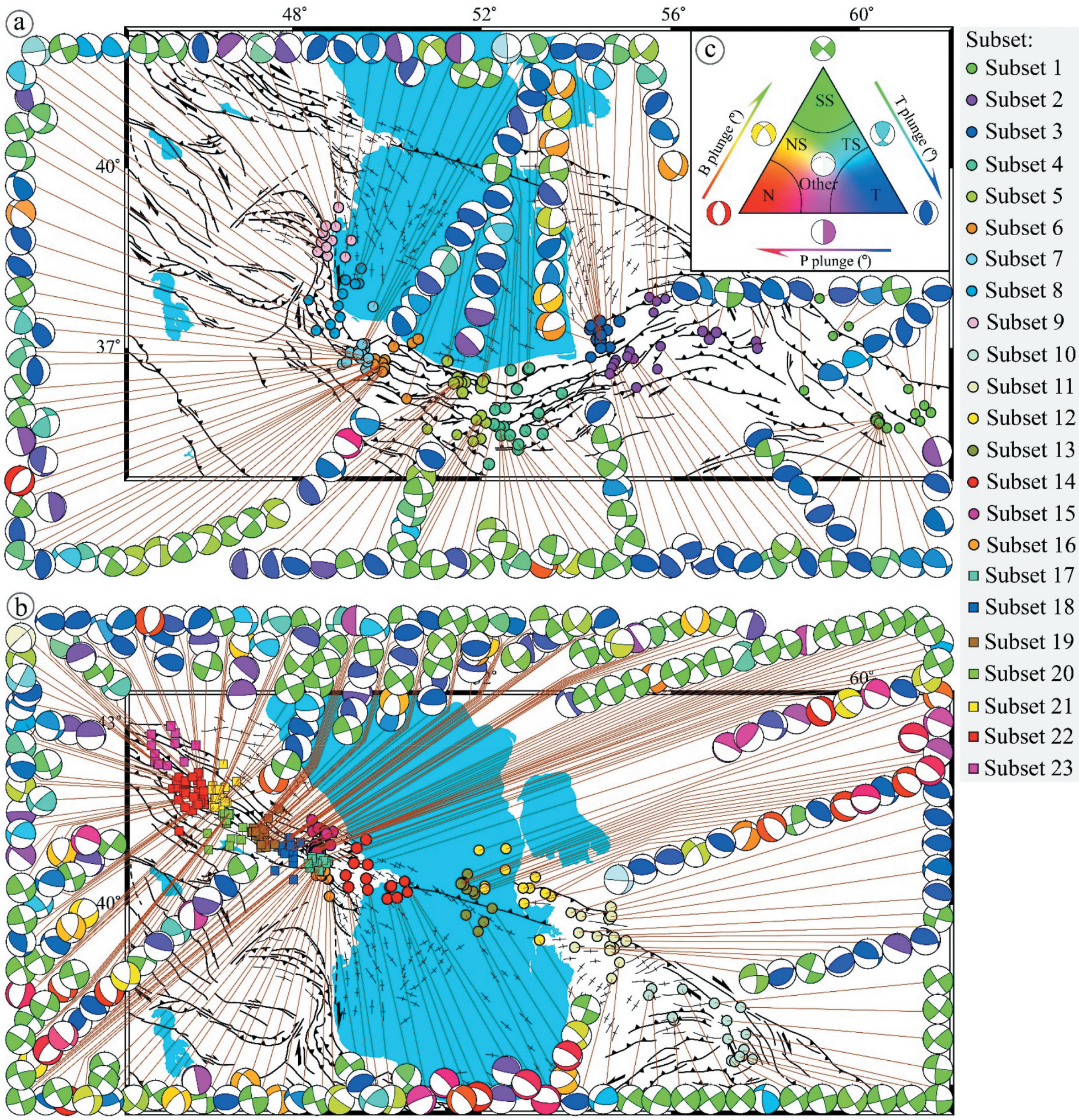

Figure 2. Spatial distribution of 410 mainshocks together with their focal mechanisms assembled into 23 subsets for the stress inversion. Colours of epicentres refer to different subsets. (a) and (b) present EFMs of subset 1 to 9 and 10 to 21, respectively. Type of the mechanisms is coloured based on the background colour of the Frohlich's triangle diagram (Frohlich 1992) presented in (c). SS: strike-slip, T: thrust, N: normal, NS: normal to strike-slip, TS: thrust to strike-slip, and other: other type of faulting.

where $\sigma_1 \geq \sigma_2 \geq \sigma_3$), and the stress ratio ϕ. The stress tensor is determined in iterations:

(1) Orientations of the principal stress axes and the stress ratio are initially determined using the Michael's method (Michael 1987) with randomly selected nodal planes as the faults.
(2) The fault instability parameter is evaluated (Lund and Slunga 1999; Vavryčuk 2011, 2014, 2015) for nodal planes of all inverted EFMs using the stress determined in step 1, and the nodal planes that display a higher fault instability are selected as the true faults. Then, the Michael's method (Michael 1987) is applied again to refine the stress.
(3) Step 2 is repeated until the process converges to the optimum final stress.

In addition, the stress inversion is run on a grid of friction values to maximize the overall fault instability.

Once the optimum stress tensor was determined, the method of Lund and Townend (2007) was used to calculate the S_{Hmax} direction, and the Simpson's index $A\phi$, (Simpson 1997) was determined. Index $A\phi$ classifies the type of faulting and the stress regime: it is 0 for the radial extension faulting/radial extensive regime, 0.5 for the pure normal faulting/pure extensive regime, 1.5 for the pure strike-slip faulting/pure strike-slip regime, 2.5 for the pure reverse faulting/pure compressive regime, and 3 for the pure compressive faulting/radial compressive regime. The value of index $A\phi$ is defined as

$$A\phi = (k + 0.5) + (-1)^k(\phi - 0.5), \tag{1}$$

where ϕ is the stress ratio showing the relative magnitude of the principal stresses (Angelier 1975, 1989)

$$\phi = (\sigma_2 - \sigma_3)/(\sigma_1 - \sigma_3), \tag{2}$$

$k = 0$, 1, and 2 for the normal, strike-slip, and reverse faulting, respectively.

4. Results

As shown in Figure 2, the mechanisms display a large variability in faulting style, except for those with normal faulting, which are mostly missing. We determined the stress for the 23 spatial subsets shown in Figure 2. The inversion results for each subset are shown in Figure 3 and Table 1 (see Supplementary file), and the orientation of the S_{Hmax} is plotted for each subset on the structural map of the region in Figure 4. The stress in all subzones can be considered homogenous based on the criteria defined in Section Data and Method. Hence, the stress inversion should yield accurate and reliable results.

The highest accuracy is achieved for the orientation of the σ_1–axis, which consistently displays small 95% confidence regions for its trend and plunge angles. In contrast, the σ_2–axis and σ_3–axis show rather high scatter and larger confidence regions in several subzones (Figure 3). The size of the confidence regions is primarily controlled by: (1) the extent and quality of the data set inverted, and (2) the stress ratio in the studied subzone (Balfour *et al*. 2011; Nouri *et al*. 2023). The effect of the value of the stress ratio on the size of the confidence regions is well-documented in subzones 4, 6, 7, and 22,

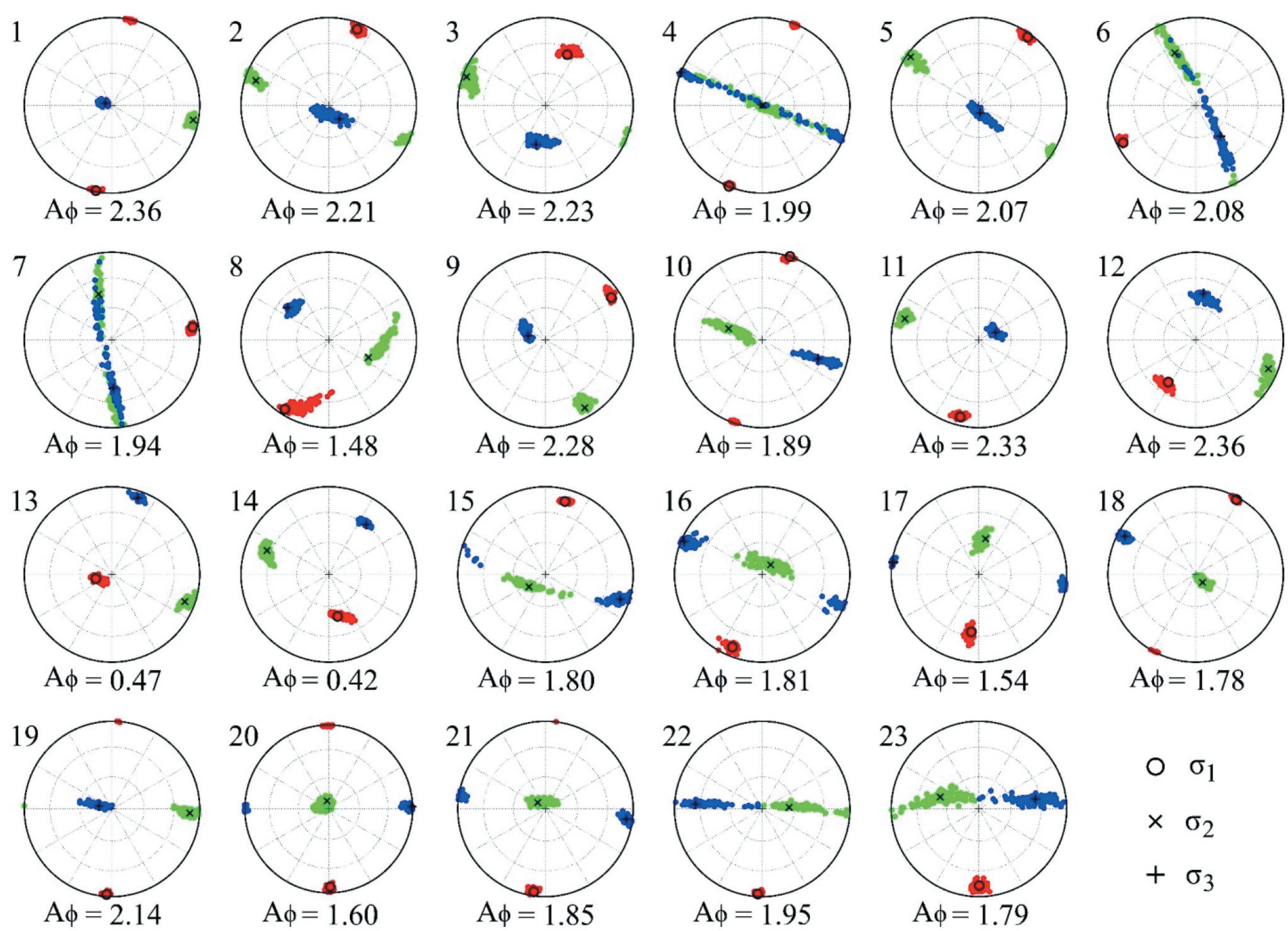

Figure 3. Stereonets of the inversion results of the 23 subsets shown in Figures 2a, b. The red, green, and blue areas indicate 95% confidence region for the σ_1, σ_2 and σ_3, respectively. The numbers in the upper-left corner of each stereonet refer to the associated subset and $A\phi$ shows stress regime.

Table 1. The results of the stress inversion for each subset presented by the principal stress axes σ_1, σ_2, and σ_3 given as trend/plunge in degree and the shape ratio ϕ. n_S: the serial number of the subset, N: the number of EFMs of the subset used in the inversion for stress, α: the deviation angle (°), and $A\phi$: the Simpson's index (Simpson 1997). The latitude and longitude of the centre of each subset is indicated by lat. and lon. respectively.

n_s	N	Lon. (°)	Lat. (°)	σ_1 (°/°)	σ_2 (°/°)	σ_3 (°/°)	ϕ	α (°)	$A\phi$	S_{Hmax} (°)
1	23	60.420	36.054	190/01	100/07	287/84	0.36	18.93	2.36	010
2	19	55.803	37.064	021/08	289/13	142/74	0.21	22.41	2.21	022
3	16	54.525	37.209	024/38	290/05	193/52	0.23	30.62	2.23	026
4	21	52.731	35.844	202/00	103/90	292/00	0.01	25.12	1.99	022
5	24	51.669	36.173	036/05	305/05	170/83	0.07	25.14	2.07	036
6	21	49.940	36.717	243/08	338/36	142/53	0.08	21.41	2.08	063
7	16	49.440	36.932	081/07	344/45	179/44	0.06	25.93	1.94	081
8	11	48.994	37.775	212/07	114/49	308/40	0.52	31.22	1.48	034
9	13	48.824	38.865	058/12	150/12	283/74	0.28	19.15	2.28	057
10	16	56.918	37.937	019/00	289/57	109/33	0.11	11.38	1.89	019
11	15	54.559	39.465	193/10	286/13	066/73	0.33	21.82	2.33	012
12	12	52.756	40.316	213/42	112/12	010/46	0.36	20.96	2.36	047
13	12	51.774	40.135	254/75	111/12	019/09	0.47	16.60	0.47	107
14	15	49.788	40.443	168/49	291/26	037/30	0.42	23.30	0.42	145
15	26	48.660	40.516	015/15	233/71	108/11	0.20	28.07	1.80	016
16	11	48.657	40.518	202.11	041/78	292/04	0.19	27.63	1.81	022
17	15	48.487	40.732	187/34	011/56	278/02	0.46	27.09	1.54	008
18	20	47.907	40.926	029/03	139/80	298/09	0.22	28.26	1.78	029
19	25	47.334	41.154	184/02	093/12	283/78	0.14	28.64	2.14	004
20	17	46.599	41.356	179/08	348/82	089/02	0.40	31.94	1.60	179
21	19	46.448	41.804	188/05	310/81	097//84	0.15	30.21	1.85	008
22	30	45.869	41.870	183/03	087/65	274/25	0.05	20.95	1.95	003
23	13	45.319	42.568	180/13	287/52	080/35	0.21	30.74	1.79	178

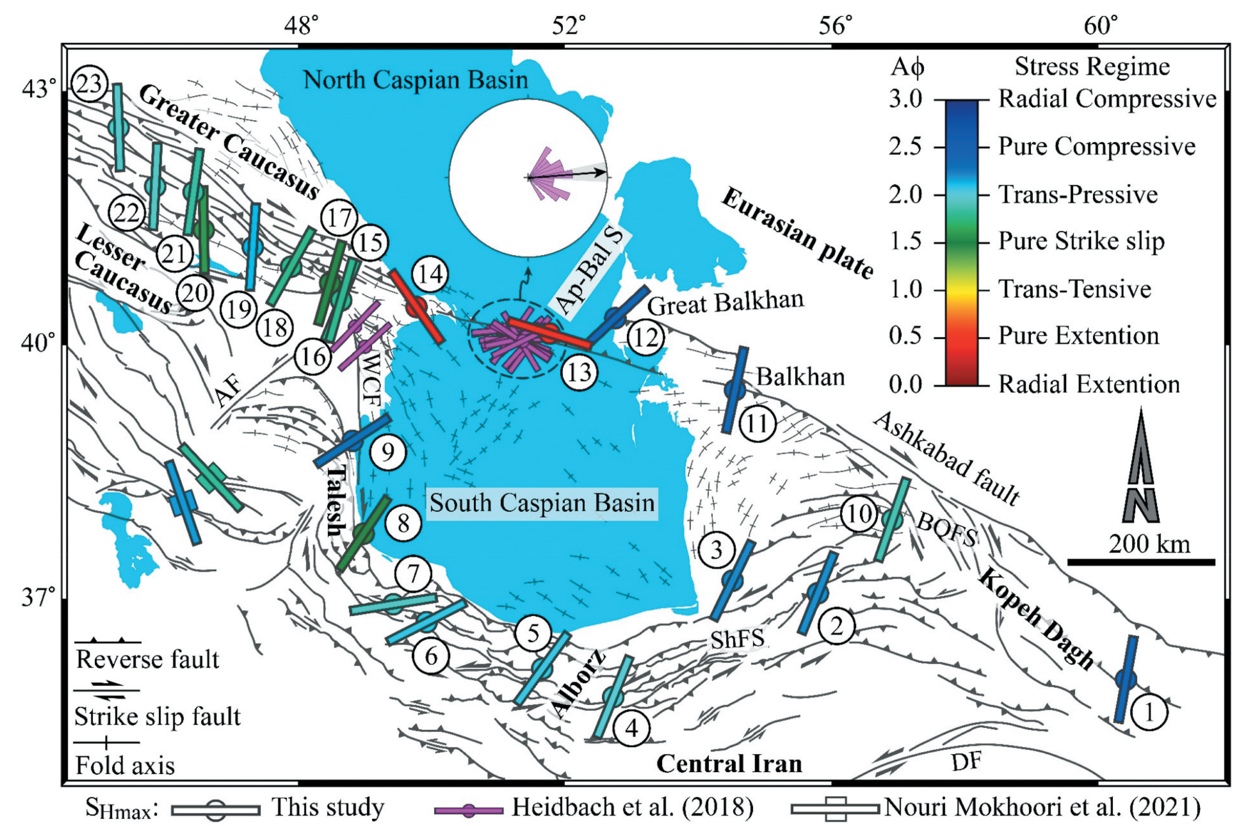

Figure 4. The S_{Hmax} for each subset plotted on structural map of the study area in centre of each subset. Colour of the S_{Hmax} indicators is based on the colour bar of the stress regime, and the related numbers refer to subsets (Figure 2). Pink bars show the S_{Hmax} orientations derived from the breakout investigations in wells (Heidbach *et al*. 2018). The rose diagram is for the borehole breakout-derived S_{Hmax}, and the arrow presents the mean orientation of the S_{Hmax}. Abbreviations have the same meaning as in Figure 1.

which are characterized by an extremely low stress ratio ($\phi < 0.1$). At the same time, their confidence regions of the σ_2- and σ_3-axes are so large that they overlap each other. Similarly, subzones 2, 10, 15, 16 and 23 display a rather low stress ratio ($0.1 < \phi < 0.2$) and their confidence regions of the σ_2- and σ_3-axes are still significantly scattered. The reason for this relation is clear: low values of ϕ indicate close magnitudes of the intermediate and minimum principal stresses and a possibility that the σ_2- and σ_3-axes can be mutually replaced.

In contrast, a high scatter of the σ_1-axis is observed for subzone 8, associated with an anomalously high stress ratio ($\phi = 0.5$), the highest value among all subzones. Obviously, since the principal stress σ_1 is less dominant than in other subzones, the confidence region of its axis is more scattered. It is worth noting that the σ_1-axis of the most subsets is close to horizontal (Figures 3, Table 1), implying the presence of a compressive stress regime. The dominance of the compressive stress is decreased by low values of the stress ratio ϕ (eq 1) (Simpson 1997).

According to the inversion results of the EFMs sets, broad consistency in orientations of the S_{Hmax} across the study area suggests that stress in the region is controlled by large-scale processes. The orientations of the S_{Hmax} can be grouped into two distinct sets (Figure 4): (1) the N to NNE orientations crossing the Greater Caucasus, and (2) the NNE to NE orientations with a few local perturbations crossing the Kopeh Dagh, Alborz, and Talesh. Regardless of the S_{Hmax} orientations, the stress regime across the study area is not of a single dominant type, and it varies from being compressive to strike-slip and to normal regimes (Figures 3 and 4, Table 1). This implies that different stress regimes are mixed in the study region. The most distinct stress state is found along the Apsheron-Balkan sill, north of the SCB.

According to the gridded stress map (Figure 5) in the central part of the Alborz, a NNE trend of the S_{Hmax} is maintained through the eastern Alborz and extends to the Kopeh Dagh fold-and-thrust belt. Toward north of this part of the region, the trend of the S_{Hmax} shows a fan-shape pattern covering the east of the SCB. Orientation of this pattern relative to the structural strikes is in agreement with kinematics of the structures. In the southwestern edge of the SCB, large changes in the orientations of S_{Hmax} are recognized, and the orientations vary from NNE in the Central Alborz to ~E-W in the Eastern Alborz. Another notable feature of the S_{Hmax} presented in Figure 5 is a large change in the orientation of the S_{Hmax} from NNE to ~E-W in the north of the SCB.

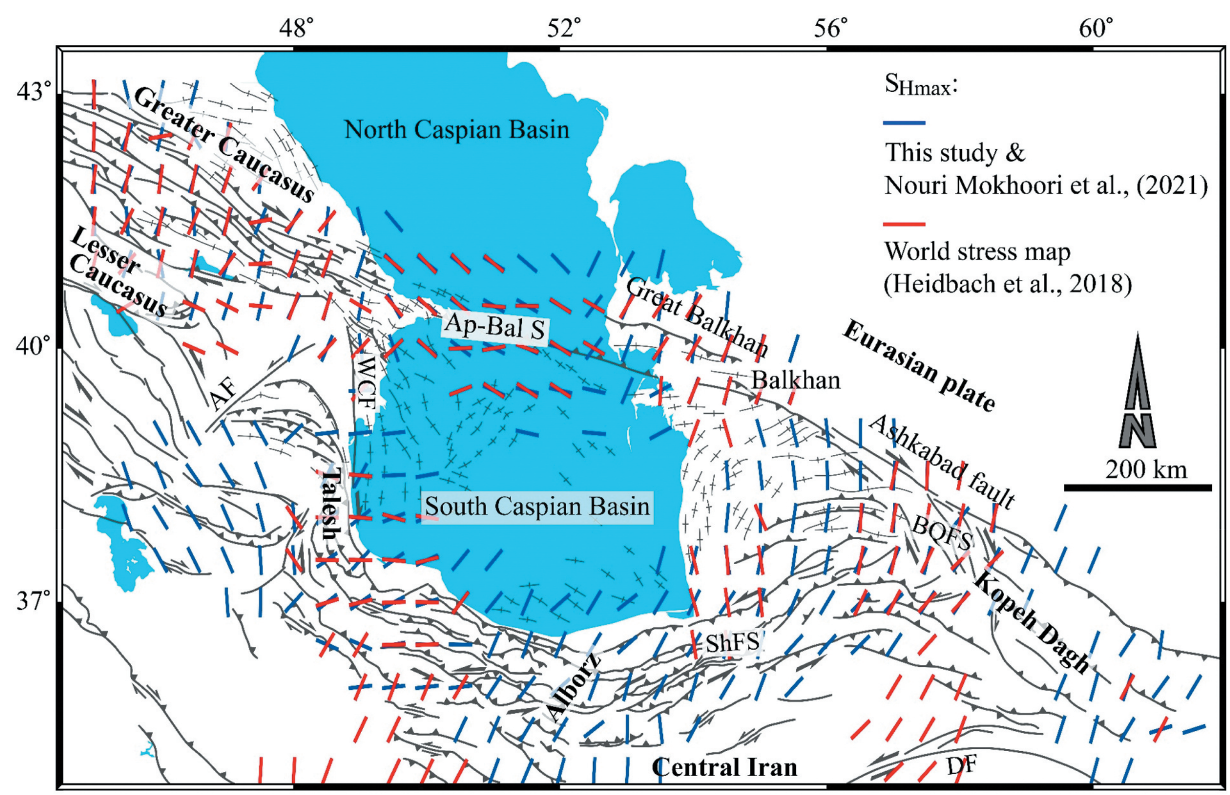

Figure 5. Mean S_{Hmax} orientation in a 0.5° grid map. The orientations are obtained by the algorithm of Carafa *et al.* (2015) on the focal mechanisms of this study and those of Nouri Mokhoori *et al.* (2021).

In the west of the Talesh, the orientation shifts counterclockwise from the NE-SW direction in the Talesh to the NW-SE direction in the NW Iran with a change in the strike of the structures, thus becoming oblique to the structures. To the north of the NW Iran, the orientation of the S_{Hmax} change to ~N in the Greater Caucasus (Figure 5).

5. Discussion

The results of the stress inversion reveal inhomogeneities in the stress field in the study region. South, east, and west of the SCB are mostly governed by transpressive stress, while the most distinct stress is detected in the north of the SCB, characterized by normal stress. We find that the S_{Hmax} within the study area is often oblique to the strike of structures. This points to the prevalence of oblique-slip movements (strike-slip and thrust), as concluded by several studies (e.g. Berberian *et al*. 1992; Lyberis 1999; Allen *et al*. 2003; Djamour *et al*. 2010; Hollingsworth *et al.* 2010, 2010; Azad et al. 2011, 2019; Tibaldi *et al*. 2020; Aflaki *et al*. 2021; Trexler *et al*. 2022; Malekzade and Bellier 2023).

5.1. S_{Hmax} orientation, $A\phi$ variation, and their relationship with active tectonics

Inversion for stress of EFM subsets across the study area reveals a variation in the S_{Hmax} orientation. The overall orientation of the S_{Hmax} is basically subparallel to the relative plate motion (Zoback 1992), which is roughly towards NNE to N. Local variations in the S_{Hmax} imply that the stress associated with plate convergence is not a single contributor to the stress field. A variety of the tectonic regimes in the region may be attributed to (1) the reactivation of old or weak faults, structural highs, flexures in the brittle crust (Priestley *et al*. 1994; Jackson *et al*. 2002; Nemati *et al*. 2013; Madanipour *et al*. 2018), and/or (2) close magnitudes of σ_2 and σ_3. The tectonics of the region is complicated by the wrapping of the Talesh-Alborz-Kopeh Dagh fold-and-thrust belt around the SCB, northward and westward subduction/underthrusting of the SCB, and the bend in the northward subducting basement of the SCB.

5.1.1. Kopeh Dagh

Seismotectonic and structural studies in the Kopeh Dagh (Tchalenko 1975; Hollingsworth *et al*. 2006; Shabanian *et al*. 2009; Walker *et al*. 2021) revealed that in addition to thrust faulting, conjugate faulting involved a right-lateral slip along NW-SE-trending main faults and a left-lateral slip along NE-SW-trending secondary faults. This pattern of faulting corresponds to the majority of focal mechanisms in subsets 1, 10 and 11 (Figure 2a, b). The mechanisms of the subset 1 are compliant with the field studies (Hollingsworth *et al*. 2010), showing that the kinematics of the southeast part of the Kopeh Dagh is marked by active thrust faulting under compressive tectonic regime with ~N-trending S_{Hmax} (N10°E) (Figure 4).

The subset 10 covers major active right-lateral strike-slip fault systems of Bakharden – Quchan and the central part of the Ashkabad fault (Figure 2b). The strike-slip fault plane solutions are closely correlated with the right-lateral active faults imaged by field studies (Hollingsworth *et al*. 2006; Hollingsworth 2007; Walker *et al*. 2021). The computed stress is characterized by the N19°E-directed S_{Hmax} (Figure 4). The same direction was found using geological fault-slip data for Late Cenozoic (Lyberis 1999). This implies that the NNE-trending stress is quite stable from Late Cenozoic to present.

According to block modelling of Mousavi *et al*. (2013), the Bakharden – Quchan fault system (BQFS) accommodates the main part of deformation in the central part of Kopeh Dagh in form of right-lateral movements and shortening at a rate of 5.2 ± 1.0 and 2.1 ± 1.0 mm/yr, respectively. Hollingsworth *et al*. (2006) estimated a ~40 km cumulative right-lateral offset for the BQFS. The main portion of the cumulated deformation in the NE Iran due to the northward motion of the Central Iran is reflected as curvature of the eastern Alborz in the east of the SCB (Figure 1) (Hollingsworth *et al*. 2010). The amount of the oroclinal bending, which took place in the eastern Alborz, was estimated to 200 ± 20 km by Hollingsworth *et al*. (2010). The BQFS cuts the eastern part of the curvature (Figure 1). Besides, the GPS measurements reveal that the Eurasian plate in the east of this fault zone is relatively stable. This points out that the BQFS has been transferred a considerable amount of deformation toward the Ashkabad fault (Figure 1).

5.1.2. Apsheron-Balkhan

Toward the northern part of the Ashkabad fault and the Great Balkhan region, the structural pattern is characterized by ~ENE to ESE-trending contractional structures (Figure 1) that are increasingly buried by sediments (Lyberis 1999). The stress computed for subsets 11 and 12 in this area indicates compressive regimes ($A\phi = 2.33$ and 2.36) with the N12°E and N47°E-directed S_{Hmax}, respectively (Figure 4). Geological studies in this region (Lyberis 1999) show that the cumulated 75 km N-S shortening over the last 5.3 Myr has been resolved into 35 km of right-lateral offset, parallel to the Ashkabad fault and 70 km of shortening perpendicular to this fault. According to Lyberis (1999), the compressional tectonic regime in this region is mainly accommodated by active folds.

In the northern part of the SCB, the tectonic activity is mainly characterized by the ~WNW-ENE-trending echelon folding and normal faulting (Figures 3 and 4) (Jackson *et al*. 2002). This indicates that the area is anomalous with respect to its eastern and western parts (Priestley *et al*. 1994; Jackson *et al*. 2002). The borehole breakout method in the central part of the Apsheron sill shows that the S_{Hmax} orientation with an average of N85°E varies from SE to NE in shallow depths (Figure 4) (Heidbach *et al*. 2018). The resulting stresses from both the eastern (13) and western (14) subsets of this region are pure extensive ($A\phi = 0.47$ and 0.42) with the ESE and NW-SE-directed S_{Hmax}, respectively. The σ_2- and σ_3-axes achieve a low value of the plunge angle relative to σ_1-axis (Figure 3 and Table 1). In such cases, the orientation of the S_{Hmax} basically follows the σ_2-axis (Lund and Townend 2007).

5.1.3. Greater caucasus

Along the Greater Caucasus, index $A\phi$ is mostly low (1.5 to 2) revealing a prevailed oblique faulting with a large component of the strike-slip faulting. The region is undergone by the N to NNE-oriented S_{Hmax} (Figure 4, Table 1). The majority of the focal mechanisms shows a right-lateral slip along the fault planes parallel to the mountain belt (Figure 2). This is supported by field studies indicating horizontal displacements across the WNW-ESE-striking thrust faults (Trexler *et al*. 2022). Therefore, the current dominant kinematics of the belt is the right-lateral transpression along the WNW-ESE-striking faults (Tibaldi *et al*. 2020).

5.1.4. Alborz

In the eastern Alborz, the S_{Hmax} and index ϕ determined for subsets 2 and 3 are similar (Figure 4, Table 1). The NNE-oriented S_{Hmax} (N22°E – N26°E) belonging to a transpressive stress regime with a high tendency toward a compressive regime ($A\phi = 2.21$–2.23) controls the kinematics of this part of Alborz. The S_{Hmax} is oblique to the strike of the structures (Figure 4), requiring left-lateral oblique-slip movements along these structures. A combination of the left-lateral and thrust movements along the Shahrud fault system covering this part of the Alborz is well studied (Hollingsworth *et al*. 2010; Hollingsworth *et al*. 2010; Javidfakhr *et al*. 2011, Javidfakhr *et al*. 2011). The GPS measurements suggest 4.5 ± 0.5 mm/yr of left-lateral slip and 1.8 ± 1.0 mm/yr of shortening across this part of the Alborz range (Mousavi *et al*. 2013).

The central part of the Alborz Mountains accommodates shortening between the Central Iran and the SCB at a rate of 8 ± 2 mm/yr (Vernant *et al*. 2004). Several mechanisms with oblique-slip faulting (mixed thrust and right-lateral) are reported in the Alborz Mountains (e.g, Jackson and McKenzie 1984; Berberian 2014). In the present study, the stress field computed for subsets 4 and 5 exhibits a horizontal axis σ_1, and σ_2 and σ_3 close in magnitude ($\phi = 0.01$ and 0.07) (Table 1 and Supplementary file). This allows permutation between axes σ_2 and stresses σ_3. Currently, the Arabian-Eurasian convergence-derived deformation along this fault system accommodates by left-lateral transpressional movements (Djamour *et al*. 2010; Azad *et al*. 2011; Rashidi 2021). Our results from 45 mechanisms (subsets 4 and 5) indicate that the transpressional tectonic regime affects the area under the ~NNE (N22°E and N36°E) S_{Hmax} (Figure 4, Table 1).

In contrast to the regional S_{Hmax} pattern, the subsets 6 and 7 in the western part of the Alborz present local variations in the S_{Hmax}, reflected in a transpressive tectonic regime ($A\phi = 1.94$ and 2.08 (Figures 2(a), 4, Table 1). The S_{Hmax} is oriented at a low angle (<45°) relative to structures maximizing the left-lateral slip of structures up to 6.3 mm/yr (Khorrami *et al*. 2019). Accompanying longitudinal structures, there is a left-lateral shear system best exemplified by the Rudbar-Tarom earthquake of 20 June 1990 Ms 7.7 (Berberian *et al*. 1992).

5.1.5. Talesh

The EFMs in the Talesh and west of the SCB show a range-parallel thrust or right-lateral oblique-slip fault planes (Figure 2a). The stress for this area is obtained from subsets 8 and 9 (Figure 2b). The subset 8 is characterized by $A\phi$ values of 1.48 and displays the strike-slip tectonic regime and faulting with the N34°E S_{Hmax} (Figure 4, Table 1). These results are consistent with right-lateral movements along the N - NNW-trending structures of the region (Barzegari *et al*. 2016; Madanipour *et al*. 2018; Azad *et al*. 2019). The same orientation of S_{Hmax} (~N40°E) is detected from geological fault-slip data in west of Talesh for Quaternary time by Aflaki *et al*. (2021). Subset 9 is associated with a compressional regime ($A\phi = 2.28$) with the N57°E S_{Hmax}. The orientations of S_{Hmax} in Talesh are in agreement with borehole breakouts in the Kura basin, north of Talesh (Figure 4) (Heidbach *et al*. 2018), however, the borehole breakout-derived S_{Hmax} is representative for shallower depths than for earthquakes. Active tectonics of Talesh is affected by (1) the NNE motion of the Talesh domain between the Aras and West Caspian faults (Vernant *et al*. 2004; Reilinger *et al*. 2006; Aktuğ *et al*. 2013; Aziz Zanjani *et al*. 2013), (2) the WNW motion of the south Caspian block and consequent underthrusting beneath Talesh (Allen *et al*. 2002, 2003; Jackson *et al*. 2002), and (3) the right-lateral movements along N-S-trending structures

(Madanipour *et al*. 2018; Azad *et al*. 2019). Such complexity can make a sharp variation in the stress field of the area (Figures 4 and 5). However, Madanipour *et al*. (2018) believed that the kinematic variation of the major faults across the Talesh must be due to change in the orientation of the S_{Hmax}.

5.2. Comparison of inversion results with previous stress studies

The S_{Hmax} pattern deduced in this study is similar to the global intra-plate stress pattern published by Heidbach *et al*. (2018) (Figure 5). Nevertheless, differences are observed in the southern part of the eastern Alborz, Talesh and some parts of the Greater Caucasus. The orientations of the S_{Hmax} do not match closely the GPS-derived principal axis of the maximum horizontal strain (e_{Hmax}) (Khorrami *et al*. 2019) as reported by Balfour *et al*. (2011). This disagreement is expected for the following reasons: (1) The e_{Hmax} mostly reflects the elastic deformation recovered during the next large magnitude earthquakes, (2) the e_{Hmax} shows local deformations, while mainshocks are produced by the regional stress, and (3) the e_{Hmax} represents rather short-period deformation, while earthquakes are connected to long-period deformation.

Zamani *et al*. (2008) analysed stress in the NE Iran including the Kopeh Dagh mountains and the Doruneh fault (Figures 1 and 4) but their study seems to suffer from several deficiencies:

(1) Duplicate mechanisms of some earthquakes were used for the stress inversion. For example, the mechanism of the 30 July 1970 (00:52:00) M 5.7 event was included in the dataset three times, each from three different sources.
(2) EFMs from different tectonic domains were compiled into a single data set, regardless of the structural patterns of those domains.
(3) Data sets related to stress domains were defined without considering distance between the epicentres of analysed earthquakes. Such partitioning of the data sets and the method used might introduce artificial variations in stress.

Lyberis (1999) calculated the N-trending compression from a population of geologically identified fault-slips. The results of our study are consistent with Shabanian *et al*. (2010) and show that the kinematics of this area is characterized by thrust faulting ($A\phi = 2.36$) in response to a compressive stress regime with the N10°E-trending S_{Hmax} (Figure 4, Table 1). This might imply that the present and past stress patterns are similar.

Our results for the eastern Alborz are consistent with Javidfakhr *et al*. (2011), who found the N19E°-oriented S_{Hmax} corresponding to a transpressive tectonic regime with a tendency toward a compressive regime ($A\phi = 2.17$). These results do not confirm the strike-slip regime ($A\phi =$ 1.66) reported by Shabanian *et al*. (2010). The subarea definition of Shabanian *et al*. (2010) did not consider differences in structural domains. The authors incorporated focal mechanisms of the NNW-SSE-trending BQFS into the those of E-W-trending arc shaped part of the Alborz. Such a dataset could lead to a biased mean stress. Our results also differ from those of Malekzade (2018), who computed a pure compressive stress regime ($A\phi = 2.6$) using only 5 focal mechanisms. Since the amount of data was low, his results were only approximate and rather unreliable. Also, Pourbeyranvand (2018) reported a more likely local rather than regional stress pattern. Since a small number of focal mechanisms and a combination of foreshock, mainshock, and aftershock focal mechanisms might produce unreliable results, we computed the stress field by using 10 or more mainshock focal mechanisms (Michael *et al*. 1990; Balfour *et al*. 2011). Recently, Malekzade and Bellier (2023) tried to determine the stress in the eastern Alborz by two sets of EFMs. They found an extensive stress ($A\phi = 0.5$) with a N100° S_{Hmax} that is not confirmed with our results and with left-lateral slips of the fault in this region.

The Arabian-Eurasian convergence in the central Alborz is accommodated by the strike-slip and thrust mechanisms or their combination (Figure 2b, subsets 4 and 5). Javidfakhr *et al*. (2011) obtained the S_{Hmax} orientation of N57°E, indicating a pure strike-slip regime ($A\phi = 1.51$) based on 8 EFMs. Malekzade (2018) analysed the stress from 3 subsets with an average of ~ 5 EFMs per subset (14 mechanisms). According to Malekzade (2018), the stress regime varies in this part of Alborz from normal ($A\phi = 0.7$) with a N150°-directed S_{Hmax} to a transpressive-strike-slip regime ($A\phi = 1.8$) with a N66° E-directed S_{Hmax} and a radial compressive stress regime ($A\phi = 2.9$) with a N103°-directed S_{Hmax}. As commonly known, the local extension can result from small pull-apart basins formed within the left-stepped zones of a left-lateral strike-slip fault, as found in NW Iran (Azad et al. 2015, 2019; Taghipour *et al*. 2018).

Recently, Malekzade and Bellier (2023, their table 1) determined the stress field for Plio-Pliestocene and Quaternary units in the central and the eastern Alborz. Their directions of the S_{Hmax} show high dispersion, the S_{Hmax} fluctuating significantly from N to N168°. In addition, they determined the stress in the central Alborz from sets of mixed EFMs. Again, their results show a large variety of the S_{Hmax} orientations (from N18° to N150°), which is not confirmed by our results.

5.3. Controls on the stress in the study area

The orientation of the S_{Hmax} in the study area varies from N to NNE in the Greater Caucasus, to NNE to NE in the Kopeh Dagh, Alborz and in the Talesh, with a few local perturbations in the eastern Alborz (Figure 4). The variation in the stress field and diversity of focal mechanisms in the study region may result from the reactivation of pre-existing structures, in particular, oblique-slip faults under laterally variable stresses (e.g, Stöcklin 1974a, 1974b; Berberian and King 1981; Berberian 1983; Priestley *et al.* 1994; Lyberis 1999; Jackson *et al.* 2002; Allen et al. 2003, 2003; Djamour *et al.* 2010; Hollingsworth *et al.* 2010; Madanipour *et al.* 2018; Naeimi *et al.* 2022; Trexler *et al.* 2022). The dominant N to NE S_{Hmax} orientations are a consequence of continental collision (Berberian and King 1981; Vernant *et al.* 2004; Reilinger *et al.* 2006) and may be traced back to the late Alpine shortening phases, as concluded by Berberian (1976) and Berberian and King (1981). This implies that the largest portion of the total stress is imposed by the convergence of large-scale tectonic plates (Heidbach *et al.* 2018).

5.3.1. Kopeh Dagh

Zamani *et al.* (2008) determined a dual stress regime with S_{Hmax} orientations of N172° and 214° for the Kopeh Dagh by automatically separating stress from EFMs. They believed that stress partitioning takes place along seismic structures. As shown in Figure 4, the orientation of S_{Hmax} in NE Iran is straightforward, following a NNE trend. Additionally, the current active faulting in the study area is likely related to the orientation of the S_{Hmax} relative to the general strike of structures. This may imply that no strain/stress partitioning has occurred in the Kopeh Dagh, as suggested by Shabanian *et al.* (2010).

5.3.2. Alborz

The EFMs along the Alborz Mountains (subsets 2 to 7) show a prevalence of thrust to strike-slip faulting (Figure 2a). The coexistence of these mixed mechanisms implies a transpressional deformation of this oblique convergence zone. In addition, some mechanisms, especially in subset 3, display a normal faulting component that indicates local extension (Figure 2a). These mechanisms are associated with the extension resulting from the bending of the basement due to the thrusting of the Alborz mountains over adjacent areas (Nemati *et al.* 2013).

The retrieved stress in the western Alborz (subsets 6 and 7) exhibits local variations. Our results show that S_{Hmax} is in the ENE direction around some faults (e.g., Rudba-Tarom fault). Probably, the stress perturbation in the eastern Alborz may not be representative for the regional stress across the study region.

5.3.3. Talesh

The left-lateral kinematics of the Aras fault and the right-lateral kinematics of the N-S-trending Talesh fault system induce the northern structural arc of the Talesh to indent (Figure 1) (Didon and Gemain 1976; Nouri Mokhoori *et al.* 2021). This may explain the compressional deformation observed in Talesh. The right-lateral movements of the Talesh fault system are not only accommodated by this indentation, as suggested in previous studies (Didon and Gemain 1976; Aziz Zanjani *et al.* 2013; Madanipour *et al.* 2018; Nouri Mokhoori *et al.* 2021) but are also transferred into the Greater Caucasus through the right-lateral movements of the West Caspian fault at a rate of 7.1 ± 0.3 mm/yr (Aktuğ *et al.* 2013). Our results do not confirm the mean S_{Hmax} provided in the World Stress Map (WSM) for the Talesh region (Heidbach *et al.* 2018). According to the WSM, the N-S-trending central part of Talesh is dominated by a NW-SE-oriented S_{Hmax}. Such an orientation of S_{Hmax} cannot account for the right-lateral kinematic on the N-S-trending Talesh fault system.

Toward the southwest of Talesh, in NW Iran, where structures are characterized by a change in the strike of the structures, the S_{Hmax} is oriented in the NW direction oblique to the strike of structures (Figure 4). The stress analysis from EFMs and geological fault-slip data in this region (Ghods *et al.* 2015; Aflaki *et al.* 2021; Nouri Mokhoori *et al.* 2021) revealed that the regional S_{Hmax} is obliquely oriented relative to NW-striking faults (Figure 4). Additionally, e_{Hmax} (Khorrami *et al.* 2019) is obliquely oriented with respect to these structures. This may be associated with the strike-slip movements across NW Iran and SE Turkey, enhancing the transfer of right-lateral movements to SE Turkey (Nouri Mokhoori *et al.* 2021). In line with these results, a recent study on paleostress during the Quaternary in NW Iran (Aflaki *et al.* 2021) reveals that σ_1 orientations follow a divergent pattern in Talesh and NW Iran. According to Aflaki *et al.* (2021), the orientations follow a NE direction in Talesh, while a NW-NNW direction in NW Iran. The divergence of the σ_1 orientations occurs approximately east of the eastern termination of the North Tabriz fault at ~ 57.5°E.

5.3.4. South Caspian basin

Dominant normal faulting under a pure extensive tectonic regime, in sharp contrast to adjacent areas, is evident in the northern part of the SCB (Figure 4). The extensional stress regime in this area can be explained by two scenarios proposed by Priestley *et al.* (1994) and Jackson *et al.* (2002): (1) This stress regime is most likely a result of the progressive plate bending that occurred in the lithosphere of the SCB, or (2) this stress regime could be related to the detachment of a sinking slab that has broken away from the Earth's surface. This stress regime is local and does not correspond to the motion between the SCB and Eurasia (Priestley *et al*. 1994; Jackson *et al*. 2002). The depth of the SCB basement varies from ~ 28 to ~33 km (Jackson *et al*. 2002). Deep earthquakes (>30 km) with a magnitude of Mw ≥ 5 are mainly concentrated in subsets 11, 12, and 13. These subsets are located along the Apsheron-Balkhan sill. This suggests that these earthquakes may originate from the bending of the subducted slab.

The results of this study, along with structural and seismotectonic studies (e.g, Berberian *et al*. 1992; Gao and Wallace 1995; Allen *et al*. 2003; Aziz Zanjani *et al*. 2013; Barzegari *et al*. 2016; Madanipour *et al*. 2018; Azad *et al*. 2019), and GPS measurements (e.g, Djamour *et al*. 2010; Aktuğ *et al*. 2013; Khorrami *et al*. 2019), allow us to propose that the southeastern edge of the South Caspian Block divides the plate convergence-derived deformation into sinistral slip along south of the SCB, Alborz, and dextral slip along west of the SCB. This suggests that the SCB should be considered an important tectonic element in the region due to its rigidity within the stressed region.

5.3.5. Greater caucasus

The structural complexity of the Greater Caucasus is reflected in the diversity of focal mechanisms (subsets 15 to 23), including variations in the type of faulting and orientation of the nodal planes (Figure 2b). This pattern of faulting suggests a complex style of deformation, including thrust faults, conjugate faults, old reactivated faults, secondary faults, and unrecognized blind and/or exhumed active faults (Tibaldi *et al*. 2020; Trexler *et al*. 2022). The majority of the mechanisms are characterized by strike-slip faulting or show a tendency toward thrust faulting. Jackson (1992) proposed that deformation resulting from the convergence between the Arabian and Eurasian plates in NW Iran, SE Turkey and the Greater Caucasus is partitioned into the right-lateral slip in NW Iran and SE Turkey and thrusting in the Greater Caucasus. However, the abundance of strike-slip mechanisms, in addition to the high tendency of the computed stress regimes toward the strike-slip type, suggests that such deformation partitioning may not occur in this region.

6. Conclusions

This paper presents an improved stress pattern around the South Caspian Basin. Our results primarily stem from stress field calculations using 10 or more mainshock focal mechanisms in individual subzones and show that the active stress and faulting styles around the South Caspian Basin are more heterogeneously distributed than previously assumed. A pure extensive stress regime is observed along the Apsheron sill associated with the bending of the South Caspian Basin basement. Thanks to the relatively high density of focal mechanisms of earthquakes along the eastern Greater Caucasus fault system, the results show that the stress is governed by transpressive to strike-slip deformation, accommodating different faulting styles. This contrasts with the contractional tectonics that is commonly considered along this fault system. In this study, for the first time, a NNE-SSW-trending strike-slip stress regime is found in the southern part of the Talesh fault system, while a NE-SW-trending compressive stress affects the northern part of this fault system. In the central and the western Alborz fold-and-thrust belt, compressive stress is combined with a strike-slip regime, while to the east, the stress exhibits a tendency toward a compressive regime.

The orientations of the S_{Hmax}, deduced from the inversion of focal mechanisms, distinguish two major domains: (1) the prevailing NNE to NE orientation is observed along the Kopeh Dagh, Alborz, Talesh, eastern Greater Caucasus, and Ashkabad-Balkhan fault zones, and (2) the dominating N to NNE orientation is present in the eastern Greater Caucasus. The results indicate that the Arabian-Eurasian convergence controls the overall stress and consequent deformation of this region.

Acknowledgments

We would like to thank the editor and two anonymous reviewers for reviews and their constructive comments that helped to improve this manuscript. We would also like to extend our thanks to Ferdowsi University of Mashhad and the Czech Science Foundation, grant No. 22-10747S (VV) for supporting this research.

Disclosure statement

No potential conflict of interest was reported by the author(s).

Funding

This study was supported by Ferdowsi University of Mashhad. One of co-authors (VV) was supported by the Czech Science Foundation, Grant No. 22-10747S.

Data and codes availability

The Centroid Moment Tensor catalogue (CMT) is available at https://www.globalcmt.org/CMTsearch.html. Other data are available from the Iranian Seismological Center (IRSC) (https://irsc.ut.ac.ir/largevents.php), the International Seismological Centre (ISC) (https://www.isc.ac.uk/iscbulletin/search/catalogue), the Kandilli Observatory and Earthquake Research Institute (https://www.koeri.boun.edu.tr), and the Zurich Moment Tensors catalogue (ZUR_RMT) (https://www.isc.ac.uk/cgi-bin/agency-get?agency=ZUR_RMT). Plotting of the focal mechanism of earthquakes on the Frohlich's diagram was performed by Orient software developed by Vollmer (2015) (https://www.frederickvollmer.com/orient/index.html). The inversion for stress was performed with open-public Matlab code STRESSINVERSE (https://www.ig.cas.cz/stress-inverse).

References

Adamia, S.A., Lordkipanidze, M., and Zakariadze, G., 1977, Evolution of an active continental margin as exemplified by the alpine history of the caucasus: Tectonophysics, v. 40, p. 183–199. doi:10.1016/0040-1951(77)90065-8.

Aflaki, M., Shabanian, E., Sahami, S., and Arshadi, M., 2021, Evolution of the stress field at the junction of talesh–Alborz–central Iran during the past 5 ma: Implications for the tectonics of NW Iran: Tectonophysics, v. 821, p. 229115. doi:10.1016/j.tecto.2021.229115.

Agard, P., Omrani, J., Jolivet, L., Whitechurch, H., Vrielynck, B., Spakman, W., Monié, P., Meyer, B., and Wortel, R., 2011, Zagros orogeny: A subduction-dominated process: Geological Magazine, v. 148, p. 692–725. doi:10.1017/S001675681100046X.

Aggarwal, C.C., and Reddy, C.K., 2014, Data clustering: Algorithms and applications: Boca Raton, Chapman and Hall/CRC, p. 652.

Aktuğ, B., Meherremov, E., Kurt, M., Özdemir, S., Esedov, N., and Lenk, O., 2013, GPS constraints on the deformation of Azerbaijan and surrounding regions: Journal of Geodynamics, v. 67, p. 40–45. doi:10.1016/j.jog.2012.05.007.

Allen, M., Ghassemi, M., Shahrabi, M., and Qorashi, M., 2003, Accommodation of late cenozoic oblique shortening in the alborz range, northern Iran: Journal of Structural Geology, v. 25, p. 659–672. doi:10.1016/S0191-8141(02)00064-0.

Allen, M.B., Jones, S., Ismail-Zadeh, A., Simmons, M., and Anderson, L., 2002, Onset of subduction as the cause of rapid pliocene-quaternary subsidence in the South Caspian basin: Geology, v. 30, p. 775–778. doi:10.1130/0091-7613(2002)030<0775:OOSATC>2.0.CO;2.

Allen, M.B., Vincent, S.J., Alsop, G.I., Ismail-Zadeh, A., and Flecker, R., 2003, Late cenozoic deformation in the South Caspian region: Effects of a rigid basement block within a collision zone: Tectonophysics, v. 366, p. 223–239. doi:10.1016/S0040-1951(03)00098-2.

Angelier, J., 1975, Sur l'analyse de mesures recueillies dans des sites failles: l'utilit ´ e d'une confrontation entre les m ´ ethodes dynamiques et ´ cinematiques: CR Academic Science Paris, v. 281, p. 1805–1808.

Angelier, J., 1989, From orientation to magnitudes in paleostress determinations using fault slip data: Journal of Structural Geology, v. 11, p. 37–50. doi:10.1016/0191-8141(89)90034-5.

Ansari, S., Yaminifard, F., and Tatar, M., 2015, Moment tensor solution of the Central-Western alborz (Iran) earthquakes based on regional data: Journal of Geoscience, v. 24, p. 359–368.

Apol'sky, P., 1974, Origin of the black and South Caspian sea troughs: Geotectonics, v. 5, p. 310–311.

Axen, G.J., Lam, P.S., Grove, M., Stockli, D.F., and Hassanzadeh, J., 2001, Exhumation of the west-central Alborz mountains, Iran, caspian subsidence, and collision-related tectonics: Geology, v. 29, p. 559–562. doi:10.1130/0091-7613(2001)029<0559:EOTWCA>2.0.CO;2.

Azad, S.S., Nemati, M., Abbassi, M.-R., Foroutan, M., Hessami, K., Dominguez, S., Bolourchi, M.-J., and Shahpasandzadeh, M., 2019, Active-couple indentation in geodynamics of NNW Iran: Evidence from synchronous left-and right-lateral co-linear seismogenic faults in western alborz and Iranian azerbaijan domains: Tectonophysics, v. 754, p. 1–17. doi:10.1016/j.tecto.2019.01.013.

Azad, S.S., Philip, H., Dominguez, S., Hessami, K., Shahpasandzadeh, M., Foroutan, M., Tabassi, H., and Lamothe, M., 2015, Paleoseismological and morphological evidence of slip rate variations along the North Tabriz fault (NW Iran): Tectonophysics, v. 640-641, p. 20–38. doi:10.1016/j.tecto.2014.11.010.

Azad, S.S., Ritz, J.-F., and Abbassi, M.R., 2011, Left-lateral active deformation along the mosha–North Tehran fault system (Iran): Morphotectonics and paleoseismological investigations: Tectonophysics, v. 497, p. 1–14. doi:10.1016/j.tecto.2010.09.013.

Aziz Zanjani, A., Ghods, A., Sobouti, F., Bergman, E., Mortezanejad, G., Priestley, K., Madanipour, S., and Rezaeian, M., 2013, Seismicity in the western coast of the South caspian basin and the Talesh mountains: Geophysical Journal International, v. 195, p. 799–814. doi:10.1093/gji/ggt299.

Balfour, N., Cassidy, J., Dosso, S., and Mazzotti, S., 2011, Mapping crustal stress and strain in southwest British Columbia: Journal of Geophysical Research: Solid Earth, v. 116. doi:10.1029/2010JB008003.

Barzegari, A., Esmaeili, R., Ebrahimi, M., Faghih, A., Ghorashi, M., and Nazari, H., 2016, Evaluation of slip rate on astara fault system, North Iran: North Iran: Journal of Earth Science, v. 27, p. 971–980. doi:10.1007/s12583-016-0680-x.

Berberian, M., 1976, Seismotectonic map of Iran: Geological survey of Iran, Tehran, scale: 1:2 500 000, 1 sheet.

Berberian, M., 1983, The southern Caspian: A compressional depression floored by a trapped, modified oceanic crust: Canadian Journal of Earth Sciences, v. 20, p. 163–183. doi:10.1139/e83-015.

Berberian, M., 2014, Earthquakes and coseismic surface faulting on the Iranian: Amsterdam, Plateau, Elsevier, p. 628.

Berberian, M., and King, G., 1981, Towards a paleogeography and tectonic evolution of Iran: Canadian Journal of Earth Sciences, v. 18, p. 210–265. doi:10.1139/e81-019.

Berberian, M., Qorashi, M., Jackson, J., Priestley, K., and Wallace, T., 1992, The Rudbar-Tarom earthquake of 20 June 1990 in NW Persia: Preliminary field and seismological observations, and its tectonic significance: Bulletin of the Seismological Society of America, v. 82, p. 1726–1755.

Bernardi, F., Braunmiller, J., Kradolfer, U., and Giardini, D., 2004, Automatic regional moment tensor inversion in the European-mediterranean region: Geophysical Journal International, v. 157, p. 703–716. doi:10.1111/j.1365-246X.2004.02215.x .

Brunet, M.-F., Korotaev, M.V., Ershov, A.V., and Nikishin, A.M., 2003, The South Caspian basin: A review of its evolution from subsidence modelling: Sedimentary Geology, v. 156, p. 119–148. doi:10.1016/S0037-0738(02)00285-3.

Cambaz, M.D., Turhan, F., Yılmazer, M., Kekovalı, K., Necmioğlu, Ö., and Kalafat, D., 2019, A review on kandilli observatory and earthquake research institute (KOERI) seismic network and earthquake catalog: 2008–2018: Advances in Geosciences, v. 51, p. 15–23. doi:10.5194/adgeo-51-15-2019.

Carafa, M.M., Tarabusi, G., and Kastelic, V., 2015, SHINE: Web application for determining the horizontal stress orientation: Computers and Geosciences, v. 74, p. 39–49. doi:10.1016/j.cageo.2014.10.001.

Chu, Y., Allen, M.B., Wan, B., Chen, L., Lin, W., Talebian, M., Wu, L., Xin, G., and Feng, Z., 2021, Tectonic exhumation across the Talesh-Alborz belt, Iran, and its implication to the Arabia-Eurasia convergence: Earth-Science Reviews, v. 221, p. 103776. doi:10.1016/j.earscirev.2021.103776.

CMT: Centroid Moment Tensor catalogue. https://www.globalcmt.org/CMTsearch.html

Didon, J., and Y.M, G., 1976, Le Sabalan volcan plio-quaternaire de l'Azerbaidjan oriental (Iran): étude géologique et pétrographique de l'édifice et de son environnement régional [Ph.D. thesis]: Grenoble, University of Grenoble, 304 p.

Djamour, Y., Vernant, P., Bayer, R., Nankali, H.R., Ritz, J.-F., Hinderer, J., Hatam, Y., Luck, B., Le Moigne, N., Sedighi, M., and Khorrami, F., 2010, GPS and gravity constraints on continental deformation in the Alborz mountain range, Iran: Iran: Geophysical Journal International, v. 183, p. 1287–1301. doi:10.1111/j.1365-246X.2010.04811.x.

Djamour, Y., Vernant, P., Nankali, H.R., and Tavakoli, F., 2011, NW iran-eastern Turkey present-day kinematics: Results from the Iranian permanent GPS network: Earth and Planetary Science Letters, v. 307, p. 27–34. doi:10.1016/j.epsl.2011.04.029.

Donner, S., Krüger, F., Rößler, D., and Ghods, A., 2014, Combined inversion of broadband and short-period waveform data for regional moment tensors: A case study in the Alborz mountains, Iran: Bulletin of the Seismological Society of America, v. 104, p. 1358–1373. doi:10.1785/0120130229.

Donner, S., Rößler, D., Krüger, F., Ghods, A., and Strecker, M.R., 2013, Segmented seismicity of the M w 6.2 baladeh earthquake sequence (Alborz mountains, Iran) revealed from regional moment tensors: Journal of Seismology, v. 17, p. 925–959. doi:10.1007/s10950-013-9362-7.

Dziewonski, A.M., Chou, T.A., and J.H, W., 1981, Determination of earthquake source parameters from waveform data for studies of global and regional seismicit: Journal of Geophysical Research: Solid Earth, v. 86, p. 2825–2852. doi: 10.1029/jb086ib04p02825.

Ekström, G., Nettles, M., and Dziewoński, A., 2012, The global CMT project 20042010: Centroid-moment tensors for 13,017 earthquakes: Physics of the Earth and Planetary Interiors, v. 200, p. 1–9. doi: 10.1016/j.pepi.2012.04.002.

Fara, H., 1964, A new catalogue of earthquake fault plane solutions: Bulletin of the Seismological Society of America, v. 54, p. 1491–1517. doi:10.1785/BSSA05405A1491.

Frohlich, C., 1992, Triangle diagrams: Ternary graphs to display similarity and diversity of earthquake focal mechanisms: Physics of the Earth and Planetary Interiors, v. 75, p. 193–198. doi:10.1016/0031-9201(92)90130-N.

Gao, L., and Wallace, T.C., 1995, The 1990 Rudbar-Tarom Iranian earthquake sequence: Evidence for slip partitioning: Journal of Geophysical Research: Solid Earth, v. 100, p. 15317–15332. doi:10.1029/95JB00320.

Ghassemi, M.R., 2005, Drainage evolution in response to fold growth in the hanging-wall of the khazar fault, north-eastern Alborz: Iran, Basin Research, Vol. 17, p. 425–436.

Ghods, A., Shabanian, E., Bergman, E., Faridi, M., Donner, S., Mortezanejad, G., and Aziz-Zanjani, A., 2015, The varzaghan–Ahar, Iran, earthquake doublet (M w 6.4, 6.2): Implications for the geodynamics of northwest Iran: Geophysical Journal International, v. 203, p. 522–540. doi:10.1093/gji/ggv306.

Granath, J.W., Soofi, K.A., Baganz, O.W., and Bagirov, E., 2007, Gravity modeling and its implications to the tectonics of the South Caspian Basin, *in* Yilmaz, P.O., and Isaksen, G.H., eds., Oil and gas of the greater caspian area: Tulsa, Oklahoma: American Association of Petroleum Geologists, pp. 1–4.

Guest, B., Guest, A., and Axen, G., 2007, Late tertiary tectonic evolution of northern Iran: A case for simple crustal folding: Global and Planetary Change, v. 58, p. 435–453. doi:10.1016/j.gloplacha.2007.02.014.

Hardebeck, J.L., and Okada, T., 2018, Temporal stress changes caused by earthquakes: A review: Journal of Geophysical Research: Solid Earth, v. 123, p. 1350–1365. doi:10.1002/2017JB014617.

Heidbach, O., Rajabi, M., Cui, X., Fuchs, K., Müller, B., Reinecker, J., Reiter, K., Tingay, M., Wenzel, F., Xie, F., Ziegler, M.O., Zoback, M.-L., and Zoback, M., 2018, The World stress map database release 2016: Crustal stress pattern across scales: Tectonophysics, v. 744, p. 484–498. doi:10.1016/j.tecto.2018.07.007.

Hollingsworth, J., 2007, Active tectonics of NE Iran [Ph.D. thesis]: Cambridge, University of Cambridge, 222 p.

Hollingsworth, J., Fattahi, M., Walker, R., Talebian, M., Bahroudi, A., Bolourchi, M.J., Jackson, J., and Copley, A., 2010, Oroclinal bending, distributed thrust and strike-slip faulting, and the accommodation of Arabia–eurasia convergence in NE Iran since the oligocene: Geophysical Journal International, v. 181, p. 1214–1246. doi:10.1111/j.1365-246X.2010.04591.x.

Hollingsworth, J., Jackson, J., Walker, R., and Nazari, H., 2008, Extrusion tectonics and subduction in the eastern South Caspian region since 10 ma: Geology, v. 36, p. 763–766. doi:10.1130/G25008A.1.

Hollingsworth, J., Jackson, J., Walker, R., Reza Gheitanchi, M., and Javad Bolourchi, M., 2006, Strike-slip faulting, rotation, and along-strike elongation in the Kopeh Dagh mountains, NE Iran: NE Iran: Geophysical Journal International, v. 166, p. 1161–1177. doi:10.1111/j.1365-246X.2006.02983.x.

Hollingsworth, J., Nazari, H., Ritz, J.F., Salamati, R., Talebian, M., Bahroudi, A., Walker, R.T., Rizza, M., and Jackson, J., 2010, Active tectonics of the east Alborz mountains, NE Iran: Rupture of the left-lateral astaneh fault system during the great 856 A.D. Qumis earthquake: Journal of Geophysical

Research: Solid Earth, v. 115, p. B12313. doi:10.1029/2009JB007185.

Hosseini, H., Pakzad, M., and Naserieh, S., 2019, Iranian regional centroid moment tensor catalog: Solutions for 2012–2017: Physics of the Earth and Planetary Interiors, v. 286, p. 29–41. doi:10.1016/j.pepi.2018.11.001.

IRSC: Iranian Seismological Center. http://irsc.ut.ac.ir/largevents.php

ISC: International Seismological Centre. http://www.isc.ac.uk/iscbulletin/search/catalogue/

Jackson, J., 1992, Partitioning of strike-slip and convergent motion between Eurasia and Arabia in eastern Turkey and the caucasus: Journal of Geophysical Research: Solid Earth, v. 97, p. 12471–12479. doi:10.1029/92JB00944.

Jackson, J., 2001, Living with earthquakes: Know your faults: Journal of Earthquake Engineering, v. 5, p. 5–123. doi:10.1080/13632460109350530.

Jackson, J., and McKenzie, D., 1984, Active tectonics of the Alpine—Himalayan belt between western Turkey and Pakistan: Geophysical Journal International, v. 77, p. 185–264. doi:10.1111/j.1365-246X.1984.tb01931.x.

Jackson, J., Priestley, K., Allen, M., and Berberian, M., 2002, Active tectonics of the south Caspian basin: Geophysical Journal International, v. 148, p. 214–245. doi:10.1046/j.1365-246X.2002.01005.x.

Javidfakhr, B., Bellier, O., Shabanian, E., Ahmadian, S., and Saidi, A., 2011, Plio–quaternary tectonic regime changes in the transition zone between Alborz and Kopeh Dagh mountain ranges (NE Iran): Tectonophysics, v. 506, p. 86–108. doi:10.1016/j.tecto.2011.04.013.

Javidfakhr, B., Bellier, O., Shabanian, E., Siame, L., Léanni, L., Bourlès, D., and Ahmadian, S., 2011, Fault kinematics and active tectonics at the southeastern boundary of the eastern Alborz (Abr and Khij fault zones): Geodynamic implications for NNE Iran: Journal of Geodynamics, v. 52, p. 290–303. doi:10.1016/j.jog.2011.02.005.

Khodaverdian, A., Zafarani, H., and Rahimian, M., 2015, Long term fault slip rates, distributed deformation rates and forecast of seismicity in the Iranian plateau: Tectonics, v. 34, p. 2190–2220. doi:10.1002/2014TC003796.

Khorrami, F., Vernant, P., Masson, F., Nilfouroushan, F., Mousavi, Z., Nankali, H., Saadat, S.A., Walpersdorf, A., Hosseini, S., Tavakoli, P., Aghamohammadi, A., and Alijanzade, M., 2019, An up-to-date crustal deformation map of Iran using integrated campaign-mode and permanent GPS velocities: Geophysical Journal International, v. 217, p. 832–843. doi:10.1093/gji/ggz045.

Khosravi, H., Javan Doloei, G., Tatar, M., and Safari, M., 2019, Analysis of the Do-Ghaleh Fariman Mw6 earthquake on 5 April 2017 and its aftershocks based on IIEES local seismic network: Journal of the Earth and Space Physics, v. 45, p. 487–505.

KOERI: Kandilli Observatory and Earthquake Research Institute. http://www.koeri.boun.edu.tr

Lentas K., 2018, Towards routine determination of focal mechanisms obtained from first motion P-wave arrivals: Geophysical Journal International, v. 212, p. 1665–1686. doi: 10.1093/gji/ggx503.

Lentas, K., Di Giacomo, D., Harris, J., and D.A, S., 2019, The ISC bulletin as a comprehensive source of earthquake source mechanisms: Earth System Science Data, v. 11, p. 565–578. doi: 10.5194/essd-11-565-2019.

Lund, B., and Slunga, R., 1999, Stress tensor inversion using detailed microearthquake information and stability constraints: Application to Ölfus in southwest Iceland: Journal of Geophysical Research: Solid Earth, v. 104, p. 14947–14964. doi:10.1029/1999JB900111.

Lund, B., and Townend, J., 2007, Calculating horizontal stress orientations with full or partial knowledge of the tectonic stress tensor: Geophysical Journal International, v. 170, p. 1328–1335. doi:10.1111/j.1365-246X.2007.03468.x.

Lyberis, N., 1999, Oblique to orthogonal convergence across the turan block in the post-miocene: AAPG bulletin: AAPG Bulletin, v. 83, p. 1135–1160. doi:10.1306/E4FD2E97-1732-11D7-8645000102C1865D.

Madanipour, S., Yassaghi, A., Ehlers, T.A., and Enkelmann, E., 2018, Tectonostratigraphy, structural geometry and kinematics of the NW Iranian plateau margin: Insights from the Talesh mountains, Iran: Iran: American Journal of Science, v. 318, p. 208–245. doi:10.2475/02.2018.02.

Malekzade, Z., 2018, Block rotation induced by the change from the collision to subduction: Implications for active deformations within the areas surrounding South Caspian basin: Marine Geology, v. 404, p. 111–129. doi:10.1016/j.margeo.2018.07.002.

Malekzade, Z., and Bellier, O., 2023, The active changeover from the transpression to the transtensional tectonic regime in eastern Alborz, Northern Iran: Journal of Asian Earth Sciences, v. 246, p. 105580. doi:10.1016/j.jseaes.2023.105580.

Mattei, M., Visconti, A.L., Cifelli, F., Nozaem, R., Winkler, A., and Sagnotti, L., 2019, Clockwise paleomagnetic rotations in northeastern Iran: Major implications on recent geodynamic evolution of outer sectors of the Arabia-Eurasia collision zone: Gondwana Research, v. 71, p. 194–209. doi:10.1016/j.gr.2019.01.018.

Michael, A.J., 1987, Use of focal mechanisms to determine stress: A control study: Journal of Geophysical Research: Solid Earth, v. 92, p. 357–368. doi:10.1029/JB092iB01p00357.

Michael, A.J., 1991, Spatial variations in stress within the 1987 Whittier narrows, California, aftershock sequence: New techniques and results: Journal of Geophysical Research: Solid Earth, v. 96, p. 6303–6319. doi:10.1029/91JB00195.

Michael, A.J., Ellsworth, W.L., and Oppenheimer, D.H., 1990, Coseismic stress changes induced by the 1989 Loma Prieta, California earthquake: Geophysical Research Letters, v. 17, p. 1441–1444. doi:10.1029/GL017i009p01441.

Mousavi, Z., Walpersdorf, A., Walker, R., Tavakoli, F., Pathier, E., Nankali, H., Nilfouroushan, F., and Djamour, Y., 2013, Global positioning system constraints on the active tectonics of NE Iran and the south caspian region: Earth and Planetary Science Letters, v. 377, p. 287–298. doi:10.1016/j.epsl.2013.07.007.

Muttoni, G., Gaetani, M., Kent, D.V., Sciunnach, D., Angiolini, L., Berra, F., Garzanti, E., Mattei, M., and Zanchi, A., 2009, Opening of the Neo-Tethys ocean and the pangea B to pangea a transformation during the permian: GeoArabia, v. 14, p. 17–48. doi:10.2113/geoarabia140417.

Nadirov, R., Bagirov, E., Tagiyev, M., and Lerche, I., 1997, Flexural plate subsidence, sedimentation rates, and structural development of the super-deep south caspian basin: Marine and Petroleum Geology, v. 14, p. 383–400. doi:10.1016/S0264-8172(96)00054-2.

Naeimi, A., Alavi, S.A., and Madanipour, S., 2022, Tectonic evolution of the foreland basin of the SE alborz mountains,

northern Iran: Journal of Asian Earth Sciences, v. 223, p. 104981. doi:10.1016/j.jseaes.2021.104981.
Nemati, M., Hatzfeld, D., Gheitanchi, M.R., Sadidkhouy, A., and Mirzaei, N., 2011, Microseismicity and seismotectonics of the firuzkuh and astaneh faults (East Alborz, Iran): Tectonophysics, v. 506, p. 11–21. doi:10.1016/j.tecto.2011.04.007 .
Nemati, M., Hollingsworth, J., Zhan, Z., Bolourchi, M.J., and Talebian, M., 2013, Microseismicity and seismotectonics of the South Caspian lowlands: NE Iran: Geophysical Journal International, v. 193, p. 1053–1070. doi:10.1093/gji/ggs114.
Niksejel, A., Shomali, Z., Cesca, S., and Moradi, A., 2021, Towards a regional, automated full moment tensor inversion for medium to large magnitude events in the Iranian plateau: Journal of Seismology, v. 25, p. 653–669. doi:10.1007/s10950-020-09967-8.
Nouri Mokhoori, A., Rahimi, B., and Moayyed, M., 2021, Active tectonic stress field analysis in NW iran-SE Turkey using earthquake focal mechanism data: Turkish Journal of Earth Sciences, v. 30, p. 235–246. doi:10.3906/yer-2011-18.
Nouri, A., Rahimi, B., Vavryčuk, V., and Ghaemi, F., 2023, Spatially varying crustal stress along the zagros seismic belt inferred from earthquake focal mechanisms: Tectonophysics, v. 846, p. 229653. doi:10.1016/j.tecto.2022.229653.
Pourbeyranvand, S., 2018, Stress studies in the central Alborz by inversion of earthquake focal mechanism data: Acta Geophysica, v. 66, p. 1273–1290. doi:10.1007/s11600-018-0207-1.
Priestley, K., Baker, C., and Jackson, J., 1994, Implications of earthquake focal mechanism data for the active tectonics of the South Caspian basin and surrounding regions: Geophysical Journal International, v. 118, p. 111–141. doi:10.1111/j.1365-246X.1994.tb04679.x.
Rashidi, A., 2021, Geometric and kinematic characteristics of the Khazar and north alborz faults: Links to the structural evolution of the north alborz-South Caspian boundary: Northern Iran: Journal of Asian Earth Sciences, v. 213, p. 104755. doi:10.1016/j.jseaes.2021.104755.
Reasenberg, P., 1985, Second-order moment of central California seismicity, 1969–1982: Journal of Geophysical Research: Solid Earth, v. 90, p. 5479–5495. doi:10.1029/JB090iB07p05479.
Reilinger, R., McClusky, S., Vernant, P., Lawrence, S., Ergintav, S., Cakmak, R., Ozener, H., Kadirov, F., Guliev, I., and Stepanyan, R., 2006, GPS constraints on continental deformation in the Africa-Arabia-Eurasia continental collision zone and implications for the dynamics of plate interactions: Journal of Geophysical Research: Solid Earth, v. 111. doi:10.1029/2005JB004051.
Rezaeian, M., Carter, A., Hovius, N., and Allen, M., 2012, Cenozoic exhumation history of the Alborz mountains, Iran: New constraints from low-temperature chronometry: Tectonics, v. 31. doi:10.1029/2011TC002974.
Ritz, J.-F., Nazari, H., Ghassemi, A., Salamati, R., Shafei, A., Solaymani, S., and Vernant, P., 2006, Active transtension inside central Alborz: A new insight into northern Iran–southern Caspian geodynamics: Geology, v. 34, p. 477–480. doi:10.1130/G22319.1.
Robert, A.M., Letouzey, J., Kavoosi, M.A., Sherkati, S., Müller, C., Vergés, J., and Aghababaei, A., 2014, Structural evolution of the Kopeh Dagh fold-and-thrust belt (NE Iran) and interactions with the South Caspian sea basin and Amu Darya basin: Marine and Petroleum Geology, v. 57, p. 68–87. doi:10.1016/j.marpetgeo.2014.05.002.
Şengör, A., 1990, A new model for the late palaeozoic—mesozoic tectonic evolution of Iran and implications for Oman, *in* Robertson, A.H.F., Searle, M.P., and Ries, A.C., eds., The geology and tectonics of the Oman: Geological society: London, Special Publications, Vol. 1, pp. 797–831.
Shabanian, E., Bellier, O., Abbassi, M.R., Siame, L., and Farbod, Y., 2010, Plio-quaternary stress states in NE Iran: Kopeh Dagh and allah Dagh-binalud mountain ranges: Tectonophysics, v. 480, p. 280–304. doi:10.1016/j.tecto.2009.10.022.
Shabanian, E., Bellier, O., Siame, L., Arnaud, N., Abbassi, M.R., and Cochemé, J.J., 2009, New tectonic configuration in NE Iran: Active strike-slip faulting between the Kopeh Dagh and binalud mountains: Tectonics, no.28. New tectonic configuration in NE Iran: Active Strike-Slip Faulting Between the Kopeh Dagh and Binalud Mountains, v. 28, p. 5. doi:10.1029/2008TC002444.
Simpson, R.W., 1997, Quantifying Anderson's fault types: Journal of Geophysical Research: Solid Earth, v. 102, p. 17909–17919. doi:10.1029/97JB01274.
Soh, I., Chang, C., Lee, J., Hong, T. K., and Park, E.-S., 2018, Tectonic stress orientations and magnitudes, and friction of faults, deduced from earthquake focal mechanism inversions over the Korean peninsula: Geophysical Journal International, v. 213, p. 1360–1373. doi:10.1093/gji/ggy061.
Stein, R.S., 1999, The role of stress transfer in earthquake occurrence: Nature, v. 402, p. 605–609. doi:10.1038/45144.
Stöcklin, J., 1974a, Northern Iran: Alborz mountains, *in* Spencer, A., ed., Mesozoic–cenozoic orogenic belts: Data for orogenic studies: Geological society: London, Special Publications, Vol. 4, pp. 213–234.
Stöcklin, J., 1974b, Possible ancient continental margins in Iran, *in* Burk, C.A., and Drake, C.L., eds., The geology of continental margins: Berlin, Springer, pp. 873–887.
Tadayon, M., Rossetti, F., Zattin, M., Calzolari, G., Nozaem, R., Salvini, F., Faccenna, C., Khodabakhshi, P., and Frassi, C., 2019, The long-term evolution of the doruneh fault region (Central Iran): A key to understanding the spatio-temporal tectonic evolution in the hinterland of the zagros convergence zone: Geological Journal, v. 54, p. 1454–1479. doi:10.1002/gj.3241.
Taghipour, K., Khatib, M.M., Heyhat, M., Shabanian, E., and Vaezihir, A., 2018, Evidence for distributed active strike-slip faulting in NW Iran: The maragheh and salmas fault zones: Tectonophysics, v. 742, p. 15–33. doi:10.1016/j.tecto.2018.05.022.
Tatar, M., and Hatzfeld, D., 2009, Microseismic evidence of slip partitioning for the Rudbar-Tarom earthquake (ms 7.7) of 1990 June 20 in NW Iran: Geophysical Journal International, v. 176, p. 529–541. doi:10.1111/j.1365-246X.2008.03976.x.
Tavakoli, F., 2007, Present-day deformation and kinematics of the active faults observed by GPS in the Zagros and east of Iran [PhD thesis]: Université Joseph-Fourier-Grenoble, 313 p.
Tchalenko, J., 1975, Seismicity and structure of the Kopet Dagh (Iran, USSR): Philosophical transactions of the royal society of London: Series A, Mathematical and Physical Sciences, v. 278, p. 1–28.
Tibaldi, A., Tsereteli, N., Varazanashvili, O., Babayev, G., Barth, A., Mumladze, T., Bonali, F., Russo, E., Kadirov, F., Yetirmishli, G., and Kazimova, S., 2020, Active stress field and fault kinematics of the greater caucasus: Journal of Asian Earth Sciences, v. 188, p. 104108. doi:10.1016/j.jseaes.2019.104108.

Trexler, C.C., Cowgill, E., Niemi, N.A., Vasey, D.A., and Godoladze, T., 2022, Tectonostratigraphy and major structures of the Georgian greater caucasus: Implications for structural architecture, along-strike continuity, and orogen evolution: Geosphere, v. 18, p. 211–240. doi:10.1130/GES02385.1.

Vavryčuk, V., 2011, Principal earthquakes: Theory and observations from the 2008 West Bohemia swarm: Earth and Planetary Science Letters, v. 305, p. 290–296. doi:10.1016/j.epsl.2011.03.002.

Vavryčuk, V., 2014, Iterative joint inversion for stress and fault orientations from focal mechanisms: Geophysical Journal International, v. 199, p. 69–77. doi:10.1093/gji/ggu224.

Vavryčuk, V., 2015, Earthquake mechanisms and stress field, *in* Beer, M., Kougioumtzoglou, I., Patelli, E., and Au, I., eds., Encyclopedia of earthquake engineering: Berlin Heidelberg, Springer-Verlag, pp. 728–746.

Vernant, P., Nilforoushan, F., Hatzfeld, D., Abbassi, M., Vigny, C., Masson, F., Nankali, H., Martinod, J., Ashtiani, A., Bayer, R., Tavakoli, F., and Chéry, J., 2004, Present-day crustal deformation and plate kinematics in the middle east constrained by GPS measurements in Iran and northern Oman: Geophysical Journal International, v. 157, p. 381–398. doi:10.1111/j.1365-246X.2004.02222.x.

Vollmer, F.W., 2015, Orient 3: A new integrated software program for orientation data analysis, kinematic analysis, spherical projections, and schmidt plots: Geological Society of America Abstracts with Programs, v. 47, p. 49.

Walker, R.T., Bezmenov, Y., Begenjev, G., Carolin, S., Dodds, N., Gruetzner, C., Jackson, J., Mirzin, R., Mousavi, Z., and Rhodes, E., 2021, Slip-rate on the main Köpetdag (Kopeh Dagh) strike-slip fault, Turkmenistan, and the active tectonics of the South Caspian: Tectonics, v. 40, p. e2021TC006846. doi:10.1029/2021TC006846.

Yetirmishli, G., Kazimova, S., and Kazimov, I., 2019, Seismic-moment tensor of earthquakes in azerbaijan for 2012–2015: Russian Geology and Geophysics, v. 60, p. 819–831. doi:10.15372/RGG2019053.

Zamani, B., Angelier, J., and Zamani, A., 2008, State of stress induced by plate convergence and stress partitioning in northeastern Iran, as indicated by focal mechanisms of earthquakes: Journal of Geodynamics, v. 45, p. 120–132. doi:10.1016/j.jog.2007.07.003.

Zoback, M.L., 1992, First-and second-order patterns of stress in the lithosphere: The world stress map project: Journal of Geophysical Research: Solid Earth, v. 97, p. 11703–11728. doi:10.1029/92jb00132.

ZUR_RMT: Zurich Moment Tensors. http://www.isc.ac.uk/cgi-bin/agency-get?agency=ZUR_RMT